# The Transarctic Acoustic Propagation Experiment and Climate Monitoring in the Arctic

Peter N. Mikhalevsky, Alexander N. Gavrilov, and Arthur B. Baggeroer, *Fellow, IEEE*

*(Invited Paper)*

***Abstract*—In April 1994, coherent acoustic transmissions were propagated across the entire Arctic basin for the first time. This experiment, known as the Transarctic Acoustic Propagation Experiment (TAP), was designed to determine the feasibility of using these signals to monitor changes in Arctic Ocean temperature and changes in sea ice thickness and concentration. CW and maximal length sequences (MLS) were transmitted from the source camp located north of the Svalbard Archipelago 1000 km to a vertical line array in the Lincoln Sea and 2600 km to a two-dimensional horizontal array and a vertical array in the Beaufort Sea. TAP demonstrated that the 19.6-Hz 195-dB (251-W) signals propagated with both sufficiently low loss and high phase stability to support the coherent pulse compression processing of the MLS and the phase detection of the CW signals. These yield time-delay measurements an order of magnitude better than what is required to detect the estimated 80-ms/year changes in travel time caused by interannual and longer term changes in Arctic Ocean temperature. The TAP data provided propagation loss measurements to compare with the models to be used for correlating modal scattering losses with sea ice properties for ice monitoring. The travel times measured in TAP indicated a warming of the Atlantic layer in the Arctic of close to 0.4 °C, which has been confirmed by direct measurement from icebreakers and submarines, demonstrating the utility of acoustic thermometry in the Arctic. The unique advantages of acoustic thermometry in the Arctic and the importance of climate monitoring in the Arctic are discussed. A four-year program, Arctic Climate Observations using Underwater Sound (ACOUS, from the Greek ακούς, meaning "listen!") is underway to carry out the first installations of sources and receivers in the Arctic Ocean. ACOUS is a joint project being executed under a bilateral memorandum of understanding with Russia and is part of the Gore-Chernomyrdin (now Gore-Primakov) Commission, Science and Technology Committee.**

***Index Terms*—Acoustic mode, acoustic thermometry, acoustic tomography, Arctic acoustics, long-range propagation, propagtion.**

Manuscript received July 8, 1998; revised December 7, 1998. This work was supported by the High Latitudes Program Office of the Office of Naval Research, by the Defense Advanced Reseach Projects Agency under the Strategic Environmental Research and Development Program (SERDP), and by the Ministry of Science and Technology Policy of the Russian Federation.

P. N. Mikhalevsky is with Ocean Sciences Operation, Science Applications International Corporation, McLean, VA 22102 USA.

A. N. Gavrilov is with the Shirshov Institute of Oceanology, Moscow 117851, Russia.

A. B. Baggeroer is with the Departments of Ocean and Electrical Engineering, Massachusetts Institute of Technology, Cambridge, MA 02139 USA.

Publisher Item Identifier S 0364-9059(99)03036-8.

## I. Introduction

IN APRIL 1994, acoustic signals were propagated across the Arctic Ocean [1], [2] to test the feasibility of using ocean acoustic tomography [3] and thermometry to provide real-time year-round monitoring of Arctic Ocean temperature and pack ice cover. The objectives of the experiment were: 1) to determine what source levels would be required to transmit over trans-Arctic Ocean ranges of several megameters and 2) to determine the phase coherence of the acoustic signals for both phase detection of CW signals and the pulse compression gain of maximal length sequences (MLS) and the consequent acoustic modal travel-time measurement accuracy. The Transarctic Acoustic Propagation (TAP) experiment demonstrated not only the feasibility of using long-range acoustic thermometry in the Arctic, but also the unique advantages associated with acoustic propagation in the Arctic half-channel for monitoring changes in the important Arctic Ocean water masses using the selective sampling of the water column by the acoustic modes. An unanticipated result of the TAP experiment was the measurement of a faster arrival time for mode 2 than was predicted using historical climatology [4], [5]. This result implied a warmer average temperture in the Atlantic layer which has been subsequently confirmed by both ice breaker and Submarine Science Ice Expediton (SCICEX) submarine conductivity–temperature–depth (CTD) transects in the Arctic. In fact, TAP, using acoustic thermometry, provided the first observation of basin-scale warming in the Atlantic layer of the Arctic Ocean.

The Arctic Ocean interacts strongly with the earth's global climate system, providing fresh water to the northern Atlantic from the surface water above the strong Arctic Ocean halocline/pycnocline, which drives the global ocean thermohaline circulation. The strong density gradient associated with the Arctic Ocean halocline/pycnocline inhibits vertical heat flux from the underlying warmer, but more saline, Atlantic water layer. This stratification is essential for maintaining the permanent ice cover in the Arctic, which in turn affects the surface albedo and the energy received by the earth–atmosphere system. It is now widely accepted that the Arctic Ocean is experiencing a weakening of the stratification and large thermohaline changes in the Atlantic layer characterized by a westward shift of the frontal region in the upper Arctic Ocean that separates the Atlantic and Pacific waters [6], [24], [7]. Little is known about what is causing these changes, and even less is known about the ultimate consequences.


Fig. 1. Transmission paths of the TAP experiment. The AO'94 icebreaker cruise and the SCICEX'95 submarine transect. The black dots on the Turpan/SIMI path are the SVP locations used in the modeling.

A full understanding of the processes that are driving these changes is limited by the inadequate observational database that exists for the Arctic Ocean. Ocean acoustic tomography and thermometry can provide a much needed real-time and year-round monitoring capability to provide cueing for more detailed icebreaker, submarine, autonomous underwater vehicle (AUV), and ice camp measurement programs as well as integrated constraints for Arctic Ocean circulation models.

The next section of the paper will describe the details of the TAP experiment. In Section III, we discuss the data analysis, signal processing, and major experimental results. In Section IV, we discuss the implications of the results of TAP for climate monitoring in the Arctic and future plans.

## II. The TAP Experiment

### A. Experiment Geometry

The TAP experiment was carried out from April 15 to April 22, 1994. During this period, there were five days of acoustic transmissions, which included 31 CW and 12 broadband acoustic signals lasting 1 h each, transmitted at a center frequency of 19.6 Hz. The signals were transmitted from a U.S./Russian ice camp "Turpan" which was drifting 300 km north of Spitsbergen in the Nansen Basin. The signals were received at the Office of Naval Research (ONR) Sea Ice Mechanics Initiative (SIMI) ice camp in the Beaufort Sea, 2600 km from Turpan, and at the U.S./Canadian ice camp "Narwhal," which was drifting at the edge of the continental shelf in the Lincoln Sea, 1000 km from Turpan. The locations of the ice camps in the Arctic Ocean are shown in Fig. 1. The coordinates of the three drifting ice camps were determined using the Global Positioning System (GPS). The positions of Narwhal and SIMI changed little during the experiment, while Turpan drifted much faster, generally southwest. The navigation tracks of Turpan, Narwhal, and SIMI are shown in Fig. 2(a)–(c), respectively. The distances from Turpan to Narwhal and SIMI were calculated using the WKS-84 geoid model [8]. The distances between the camps during the experiment are shown in Fig. 3.

### B. Acoustic Source Characteristics

The acoustic source of an electromagnetic design [9] was built for the TAP experiment at the Institute of Applied Physics in Nizhny Novgorod, Russia. Fig. 4 is a color photo of the source on the ice. The source weighs 850 kg in air and has a positive buoyancy of about 200 kg in water. The diameter of the source membrane was 1.4 m. The source design required pressure compensation, which was controlled by means of a pipe connecting the source to a high-pressure air compressor placed on the ice. The source was deployed at a depth of 60 m under the ice. At this depth, the resonant frequency of the source was measured to be 19.6 Hz. The bandwidth of the source was $\pm 1.3$ Hz at the $-3$-dB level. The source level was nominally 195 dB re 1 $\mu$Pa at 1 m (251-W acoustic power).

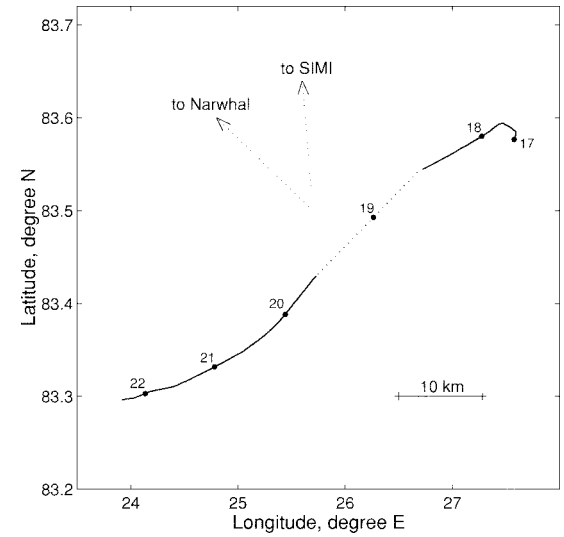


(a)

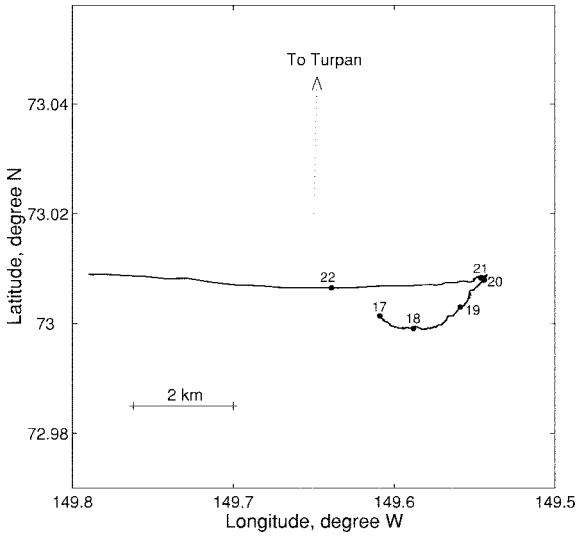


(b)

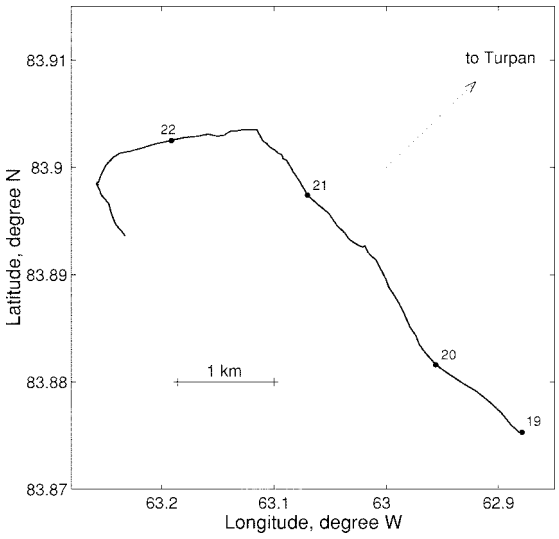


(c)

Fig. 2. The drift tracks measured using GPS of the ice camps. (a) Turpan, the source camp north of Svalbard. (b) SIMI, the Sea Ice Mechanics Initiative receiver camp north of Alaska. (c) Narwhal, the receiver camp in the Lincoln Sea.

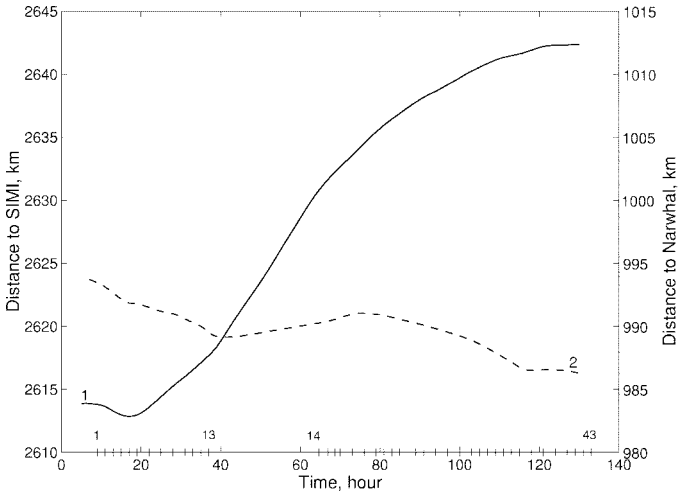


Fig. 3. Geodesic ranges from Turpan to SIMI (#1, solid line, left margin scale) and Turpan to Narwhal (#2, dotted line, right margin scale).

The level of the transmitted signal was monitored periodically by taking a vertical section of the sound pressure field using a single desensitized hydrophone which was 100 m distant from the source and suspended from a winch and lowered to 180 m. These measurements verified the transmitted levels and were used for estimating the transmission losses to the two receiving camps. Fig. 5 shows an example of the CW pressure versus depth, showing the near-field interference pattern of the direct path and the reflected path from the underside of the ice. During the 1-h transmission, the source level decreased slowly to a maximum loss of approximately 0.5 dB. The decline in the signal level was due to warming of the radiator core, causing a slight distortion of the pressure compensation system resulting in a small shift of the resonant frequency.

### *C. Transmitted Signals*

The source was driven by a signal generator which was synchronized to a rubidium clock generating a 5-MHz signal and initialized with GPS and a frequency synthesizer producing a signal at 88.4 Hz, or four times carrier frequency. The output signal of the generator could be either CW at the 19.6-Hz carrier or digitally phase-modulated with a deflection $\pm\pi/4$, which leaves half the power in the carrier. The phase modulation was controlled by an MLS generator synchronized with the carrier signal. The MLS generator was initially in a zero-state position, which corresponded to the CW signal to be generated. The start of the MLS generation was controlled manually. The duration of the MLS digit could be selected to be either 25 or 12.5 periods of frequency, which corresponds to a signal bandwidth $2/T = 2f_o/N$ of either 1.5 or 3 Hz, respectively. The length of MLS's in the TAP experiment were 127, 255, 511, or 1023 digits, which were then repeated to fill the 1-h transmission. Fig. 6 illustrates the complex demodulated amplitude and phase of a signal from the reference hydrophone. (The phases were not shifted at points of phase continuity which produced "instantaneous" fades in the amplitude. These contributed a small nonlinear component in the modulated signal which had no significant impact upon received data.) All the transmissions were on a

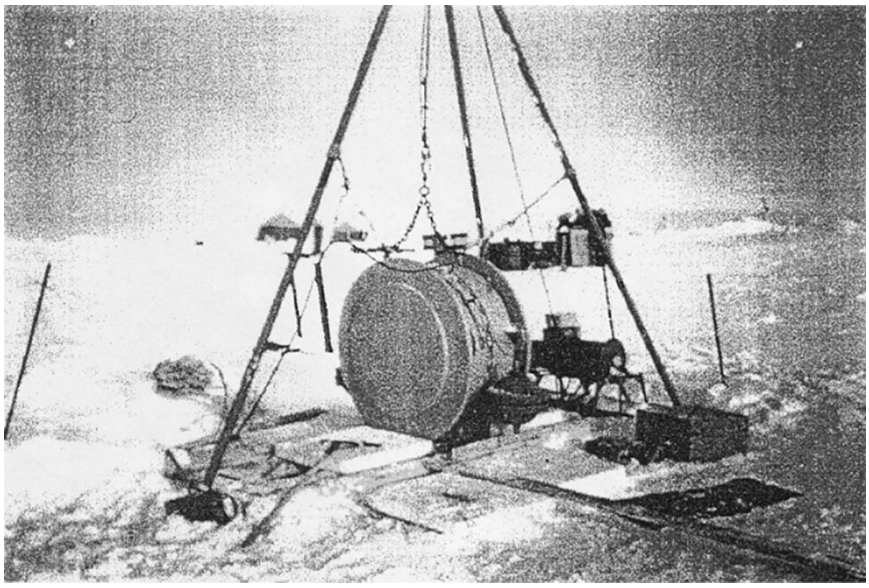

Fig. 4. Photograph of the Institute of Applied Physics 195-dB acoustic source.

regular schedule with 1 or 2 h between each transmission. Eight CW and two MLS (M255/25 and M511/25, 25 carrier cycles per digit) signals were transmitted during the first day of the experiment. On April 18, the transmissions were suspended due to technical problems with the source diesel power generator. The operation of the rubidium clock was also temporarily discontinued. Regular transmissions were resumed the next day. There were 22 CW and 10 MLS (five M255/12.5, two M127/12.5, two M511/12.5, and one M1023/12.5) signals transmitted during April 19–22, for a total of 30 CW and 12 MLS signals during the whole TAP experiment.

### *D. SIMI and Narwhal Arrays and Recordings*

At SIMI, the TAP signals were received with a linear vertical line array (VLA) and a two-dimensional (2-D) horizontal array (HA). The vertical array consisted of 32 hydrophones spaced at 7-m intervals from a depth of 62 to 279 m. The horizontal deviation of the VLA hydrophones was tracked with four acoustic beacons deployed at 60 m under the ice. The HA included 32 hydrophones suspended at a depth of 60 m and distributed as shown in Fig. 7. The signals from the VLA and HA hydrophones were sampled at 1 kHz and stored on Exabyte tapes. The sampling rate was derived from a 1-MHz time base of a GPS receiver which was phase-locked to GPS time.

The VLA deployed at Narwhal spanned almost all the water column to a depth of 530 m. The TAP signals were received at 18 VLA hydrophones. Sixteen of them were spaced at 30.2 m, while the other two hydrophones were suspended from the ice near the bottom hydrophone of the VLA with a horizontal offset. The shape of the array was monitored with an Array Element Localization (AEL) system which consisted of four acoustic transponders deployed under the ice around the array and three AEL receivers installed on the array at the top, middle, and bottom. The signals from the VLA were sampled at 256 Hz, and the accompanying data were also recorded on Exabyte tapes. A GPS time clock was also used for the time

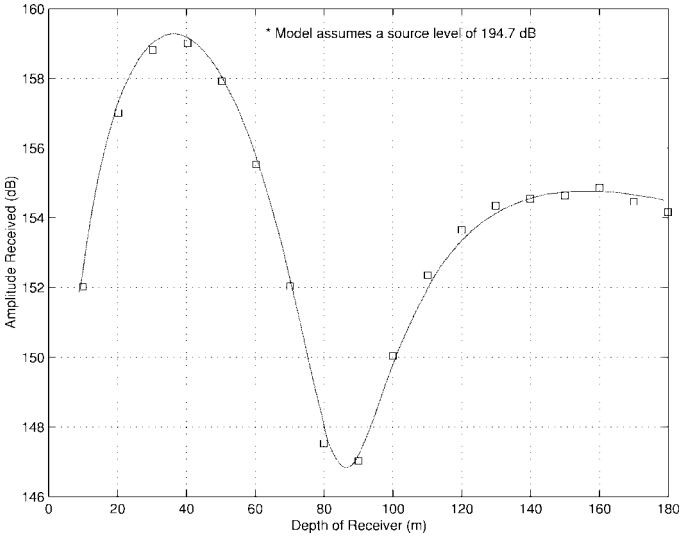


Fig. 5. Sound pressure level versus depth from source monitor hydrophone. The squares are the measured data points and the red line is the modeled result, yielding a source level measurement of 194.7 dB for this CW transmission.

synchronization of the recordings. A complete description of the Narwhal data may be found in Pawlowicz *et al.* [10].

### *E. TAP Environmental Data*

CTD profiles were measured at Turpan and Narwhal several times during the period of the TAP transmissions. At SIMI, the vertical soundings of the water column included only the temperature due to a problem with the CTD. Sound velocity profiles (SVP's) for SIMI were subsequently calculated using LEADEX 92 salinity data taken in the same season and region. Typical sound-speed profiles taken at Turpan, SIMI and Narwhal are shown in Fig. 8. For acoustic modeling of the propagation along the TAP paths to represent the historical climatology, we used the generalized digital environmental model (GDEM) and Russian POLEX databases for the tem-

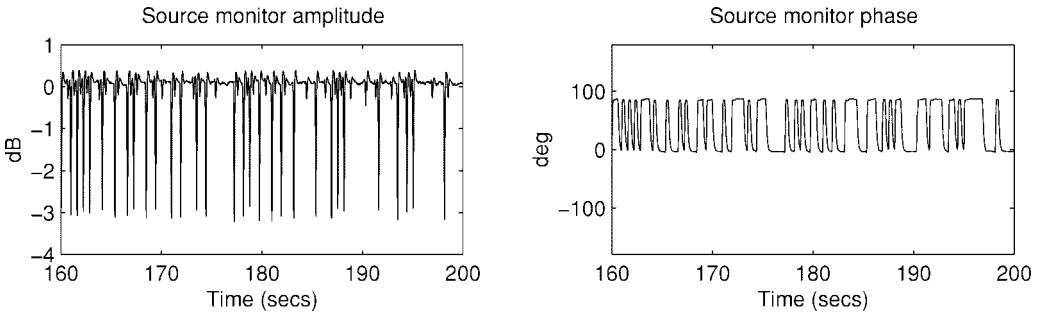


Fig. 6. Amplitude and phase of the transmitted signal recorded on the source monitor hydrophone and complex demodulated at the 19.6-Hz carrier frequency.

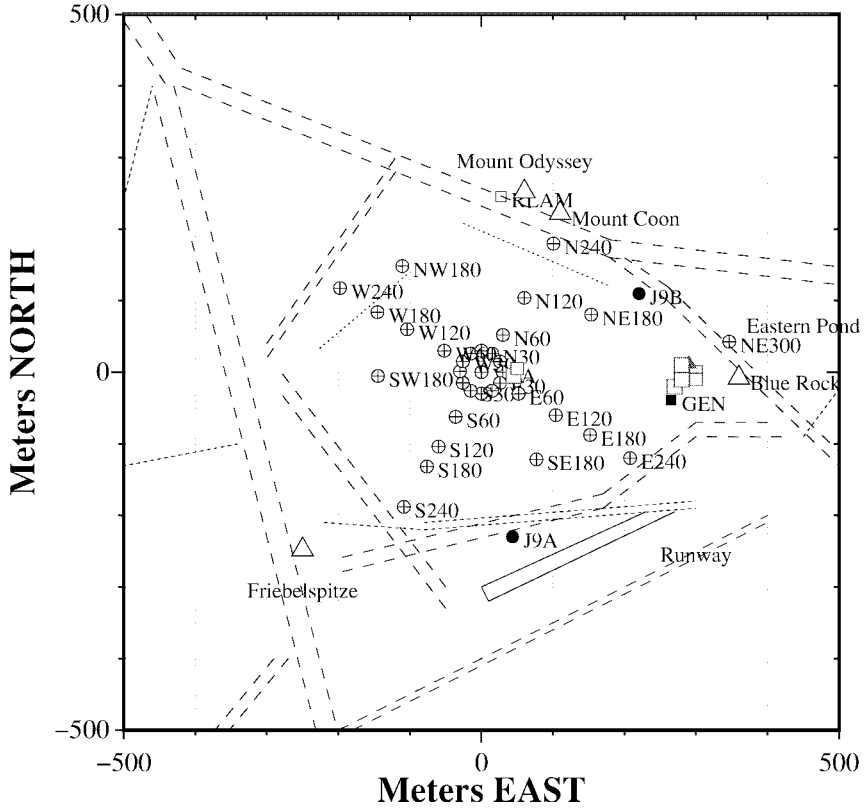


Fig. 7. The layout of the SIMI ice camp indicating the locations of the 32-element horizontal and vertical arrays. The circles with crosses show the actual hydrophone positions, with the letters indicating geographic direction and the numbers indicating the range in meters from the center of the array where the vertical array is located. The black dots are the J9 acoustic sources, and the triangles are various ice and pressure ridge features around the camp.

perature and salinity fields in the Arctic Ocean [11], [12]. The model of the sound-speed profiles and bathymetry along the TAP paths, respectively, shown in Fig. 9(a) and (b) for Turpan–SIMI and Turpan–Narwhal, has been derived from the 5-min topography grid of the Earth surface [13].

## III. Acoustic Receptions, Data Processing, and Modeling

### *A. CW Signals*

The CW data received at SIMI were processed using a three-stage demodulation and low-pass filtering routine resulting in a complex envelope signal with a 14-MHz bandpass centered on the carrier at 19.6 Hz. Fig. 10(a) compares the predicted phase change at 19.6 Hz recorded for a VLA phone at a depth of 62 m, caused by the relative motion between Turpan and SIMI using the GPS navigation with the measured phase from the CW transmissions and the carrier component of the MLS transmissions. Because the transmissions were not on continuously, there is a phase ambiguity from one transmission to the next; however, exact start and stop times are known, so the acoustic phase was aligned in time with the navigation and then shifted up or down to match the navigation. Fig. 10(a) shows the phase extracted from the carrier component for all the transmissions on April 17 from 0800Z to 2400Z, while Fig. 10(b) shows the same for April 20 from 0000Z to 2400Z. The acoustic phase and the drift phase within each segment match very closely, as well as closely tracking the up and down Doppler shift [Fig. 10(a)] as the camps opened and closed range. This provides compelling evidence that the phase changes were clearly dominated by the relative camp drifts. Fig. 11(a) is an expanded plot of the phase of the April

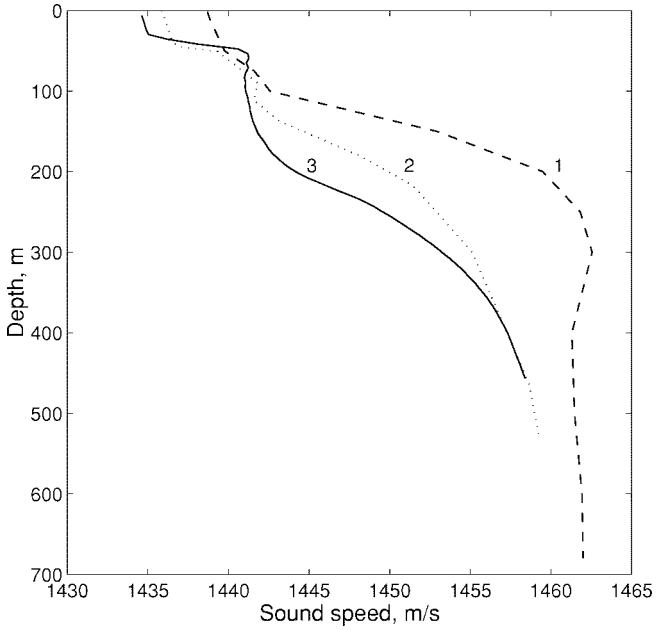


Fig. 8. Sound-speed profiles measured at the ice camps. 1) Turpan, the source camp north of Svalbard. 2) SIMI, the receiver camp north of Alaska. 3) Narwhal, the receiver camp in the Lincoln Sea.

20 1100–1200Z CW transmission [Fig. 10(b)], before and after removal of the phase shift due to the camp drift. [Since the time shown in Figs. 10(a) and (b) are the receive times, the April 20 1100–1200Z transmission starts at 1100Z plus the transmission time of just over 30 min or approximately 1130Z on Fig. 10(b).] Fig. 11(b) has been further expanded showing the phase after removal of the camp drift. The exceptional phase stability at low frequencies of the Arctic Ocean propagation has been observed previously, but those earlier measurements were made at only a few hundred kilometers [14]. The TAP experiment has shown that this stability is supported at transbasin ranges. The standard deviation of the phase shown in Fig. 11(b) is 0.01 cycles or 0.75 m. Following Mikhalevsky [14], we can assume that the phase fluctuations evidenced in Fig. 11(b) are due entirely to in-band noise. This Rician model assumes that the relative phases of the multimode reception remain constant over the hour of the transmission. Given the exceptionally small fluctuations, this is a good assumption. The postprocessing signal-to-noise ratio (SNR) of this transmission was 26 dB. For a Rician process, this yields a phase standard deviation of 0.008 cycles, which indeed accounts for all of the observed phase variance. Alternatively, the measured 0.01 cycle standard deviation implies that the standard deviation for the measured travel-time changes along the propagation path is 0.5 ms which corresponds to average temperature changes along the path of 0.1 m°C. As explained in Section IV-A1 below, this measurement accuracy is over an order of magnitude better than is required for long-term ocean temperature monitoring.

Over long observation times, and with the consequent changes in the water mass temperatures, the multimodal phase intereference inherent in the long time average CW detection will probably cause phase changes difficult to interpret and invert. It is necessary, therefore, to separate the modes and monitor their phases individually. This can be done using a VLA of sufficient length (≈1500 m in deep water to resolve modes 1–5). Alternatively, the temporal dispersion of the lowest modes can be exploited to separate the modes in time using the "wide-band" MLS signals.

### *B. MLS Signals*

As indicated above, each MLS consisted of a repetition of a 127-, 255-, 511-, or 1023-digit code for an hour. The first two MLS transmissions used 25 cycles of the 19.6-Hz carrier frequency (≈1.28 s) per digit, while the remaining 10 used 12.5 cycles (≈0.64 s) per digit. The MLS data were low-pass filtered, downsampled, and then replica correlated. The complete algorithm for processing the MLS signals on the horizontal array is given by the following:

1) beamforming to obtain 8–10 dB of array gain;
2) complex envelope demodulation;
3) phase correction for the Doppler shift induced by the relative drift of the ice camps;
4) pulse compression;
5) carrier suppression;
6) coherent sequence averaging (except for the first and last sequences).

(See Appendix A for the signal model.) Fig. 12 shows the entire 1-h signal of transmission #23 after pulse compression. The sharp peaks correspond to a group of modal arrivals which are separated by one complete period of the 255-digit sequence (≈162.6 s). The processing gain for one period is ≈21 dB, which is given by $10\log(N)$ where $N$ is the sequence length of the MLS, less 3 dB, since the phase modulation left half the energy in the carrier. After the pulse compression, $K$ sequences are coherently summed over the hour after compensating for the camp drift by adjusting the phase of each sequence. This provides $10\log(K)$ gain. Fig. 13 illustrates the coherent and incoherent signal processing results for transmission #23. Note the SNR for a single period (indicated by the black line) is ≈20 dB. Coherent summation for 10 and 20 sequences, shown by the red and green lines, respectively, provides an additional gain very close to the 10–13-dB theoretical limit. This is one of the important results of the TAP experiment. After 2600 km of propagation across the Arctic Ocean and continual reflection and scattering from the pack ice, all of the MLS's still retained their phase coherence over the full hour, which led to near optimal pulse compression and coherent processing gains at 19.6 Hz.

At SIMI, the MLS data were beamformed on the 32-element HA prior to pulse compression and coherent summation. Fig. 14 shows the beamformed pulse-compressed coherently summed arrival structure for transmission #23, the 255-digit MLS discussed above. A predicted received signal using the range-dependent coupled-mode code of Evans [20] modified by Freese [21] with the GDEM model is also shown. The comparison of the arrival times will be discussed below.

Pulse compression and coherent summation were also performed on each channel of the VLA at SIMI. The arrival structure as a function of depth from the VLA was used to unambiguously associate the pulse compressed peaks with the

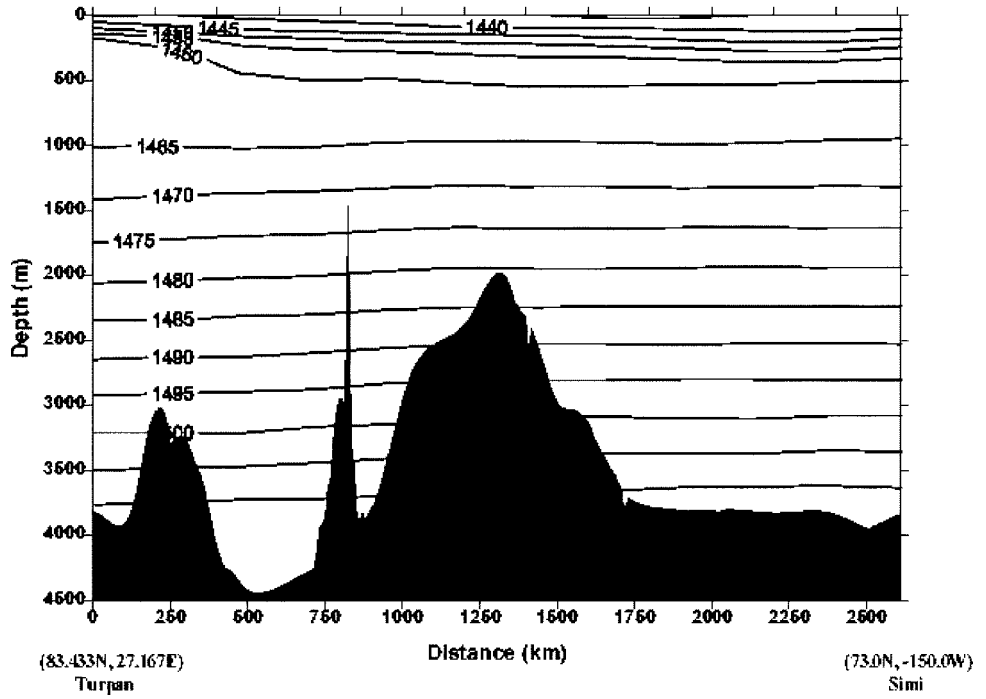


(a)

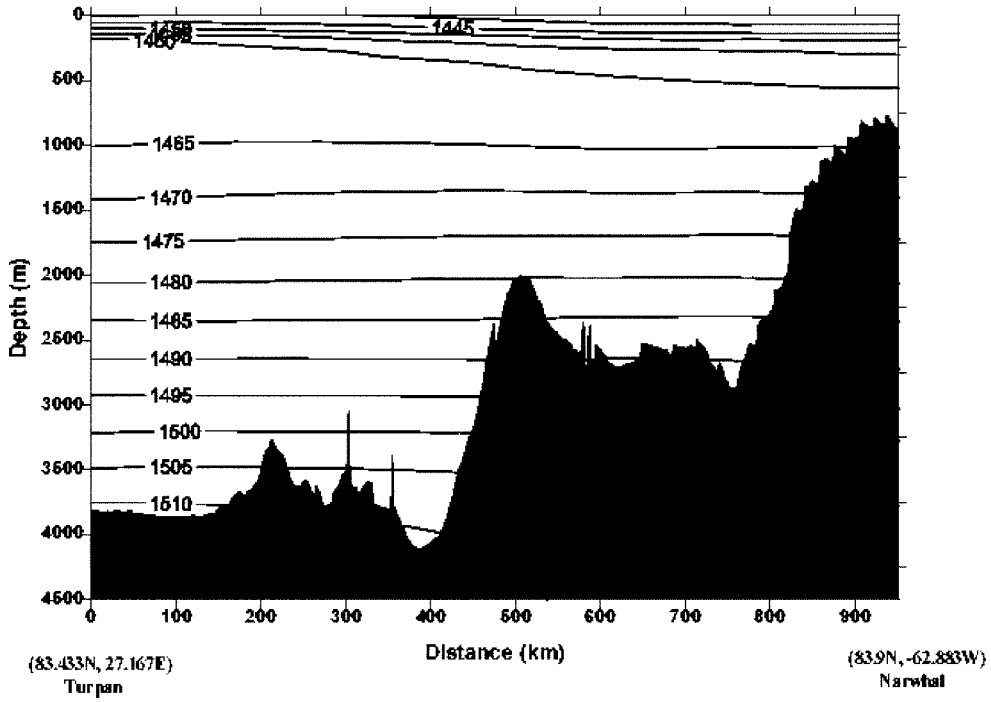


(b)

Fig. 9. Sound-speed profiles and bathymetry along propagation paths. (a) Turpan–SIMI. (b) Turpan–Narwhal.

modal arrivals for modes 2–4. The upper left panel of Fig. 15 shows the HLA beamformed result (the same as shown in Fig. 14), and the lower left panel shows the arrivals on each channel of the VLA plotted as a function of depth. At each of the arrival times of the three sharp peaks on the HA, the amplitude pattern on the VLA has nulls at a well-defined depth. The depths correspond to the zeroes of modes 2–4 computed using the CTD data from SIMI. The mode shapes are plotted in the right panel of Fig. 15. Mode 1 is not observed on a single VLA channel and was not observed after HA beamforming for four of the 12 MLS transmissions due to its much higher ice scattering losses (see below). The wide peak arriving before mode 4 in Figs. 14 and 15 is a combination of higher order modes which have travel times too close to be resolved; in addition, these modes interact with the Lomonosov Ridge which extends to within 2000 m of the

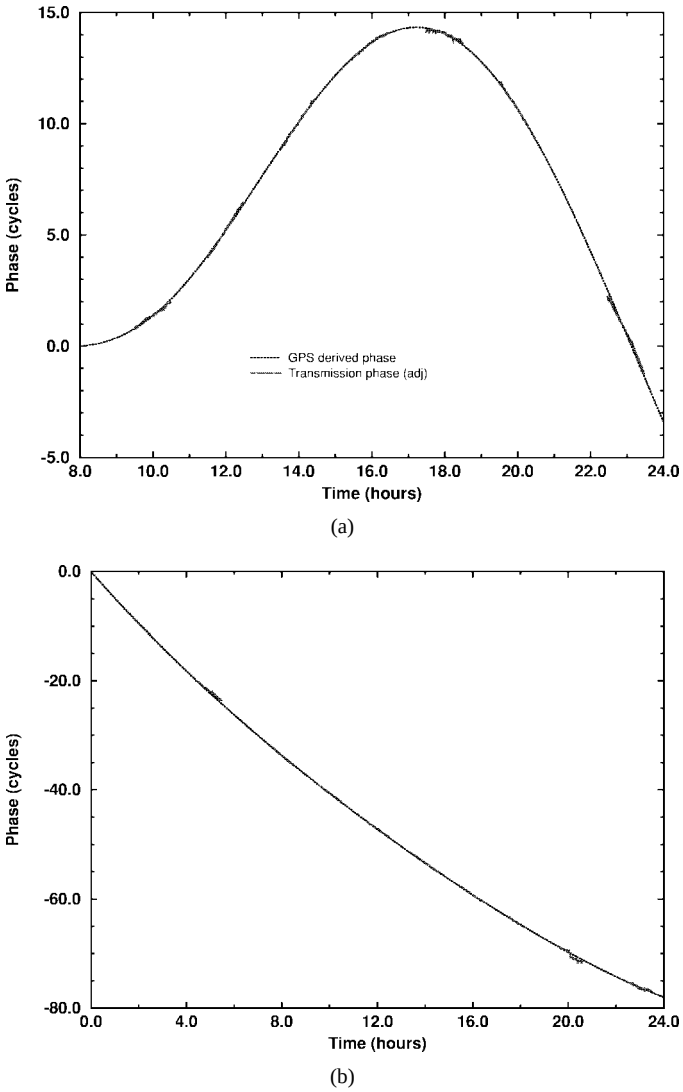


Fig. 10. Phase of two segments separated by three days compared to the corresponding GPS navigation. (a) April 17, 0800Z to 2400. (b) April 20, 0000Z to 2400Z. The blue line represents the phase change due to the GPS-derived relative camp drift, and the red lines are the phase changes derived from the acoustic transmissions.

surface, causing significant modal coupling, and makes their interpretation difficult. Normal mode propagation modeling suggests that modes higher than 10 are effectively stripped out by the Lomonosov Ridge. As discussed below, however, for Arctic Ocean monitoring, the low-order modes (1–4) are the most important since they selectively sample the water column at depths of the important water masses.

### *C. Travel-Time Measurements and Models*

The recent CTD measurements taken by icebreakers CCGS Henry Larsen in August–September 1993, the joint expedition of the USGS Polar Sea and the RCV Louis S. St. Laurence in August 1994 (AO'94), and by the submarine USNS Cavalla (SSN-684) in April 1995 (SCICEX'95) show an intrusion of warmer Atlantic Intermediate Water (AIW) in the eastern Arctic and beyond the Lomonosov Ridge in the Makarov Basin in contrast to the historical climatology [15]–[17]. Modeled travel times and interarrival times using these data agree more closely with TAP measured results. The increase in temperature inferred from the TAP observed travel-time changes between the data and the model using the historical climatology is consistent with the change in the CTD measurements. These results demonstrate the value and potential of acoustic thermometry as an effective method for long-term synoptic observations of temperature changes in the Arctic Ocean. In fact, this was the first instance where acoustical measurements anticipated direct oceanographic sampling.

The experiment not only showed that it is possible to measure the integrated temperature change along the path with a precision approaching 0.1 m°C, it also detected average warming along the path in the AIW (200–700 m depth) of approximately 0.4 °C [4], [5]. This temperature change was inferred from observed differences in the travel time of acoustic mode 2, which is most sensitive to temperature changes in the AIW layer as compared to that predicted using historical climatology [4], [18]. Direct measurements using CTD's deployed from icebreakers have shown an increase in temperature of the AIW in the Makarov Basin [15] and in the eastern Arctic [16] when compared to earlier measurements. This result was affirmed again in April 1995 during the cruise of the submarine USS Cavalla during the SCICEX'95 experiment in which 68 submarine-launched, under-ice, expendable conductivity, temperature, and depth (SSXCTD) probes were deployed on a track from the Beaufort Sea to Franz Josef Land [17]. These new measurements showed temperature differences with the historical climatology that are consistent with the acoustically derived results of TAP. Using sound-speed profiles from the Arctic Ocean icebreaker cruise of August 1994 (AO'94) and those we obtained from the SCICEX'95 cruise, we have performed additional acoustic modeling that yield results that are in better agreement with the experimental measurements from TAP. The remaining differences between these new model results and the TAP data reflect the fact that the sound-speed profiles from AO'94 and from SCICEX'95 were not exactly coincident with the TAP propagation track in space or time; however, it will be important for future experiments that simultaneous measurement of SVP's along acoustic propagation paths be performed at least once to provide a better baseline than we were able to achieve with the TAP experiment.

*1) Travel Time and Phase Measurements:* The source transmissions at the transmitter were regulated by a rubidium oscillator, which was manually synchronized to absolute GPS time at the beginning of the experiment, and once again after a casualty to the camp generator forced a shutdown of all electronic equipment. The receivers at the SIMI and Narwhal were synchronized continuously to GPS. The largest timing error was associated with the manual sychronization to GPS at Turpan, and this was estimated to be nominally 1 s. The ranges between the source and receiver camps were determined by GPS for each of the 12 MLS transmissions. Nominal positional errors are 30 m corresponding to 20 ms, and averaging with the slow camp drifts reduced this further. Differential timing errors during a transmission are estimated to be less than 1 ms. The absolute travel time was measured by detection of the peak of each of the resolved modes (1–4)

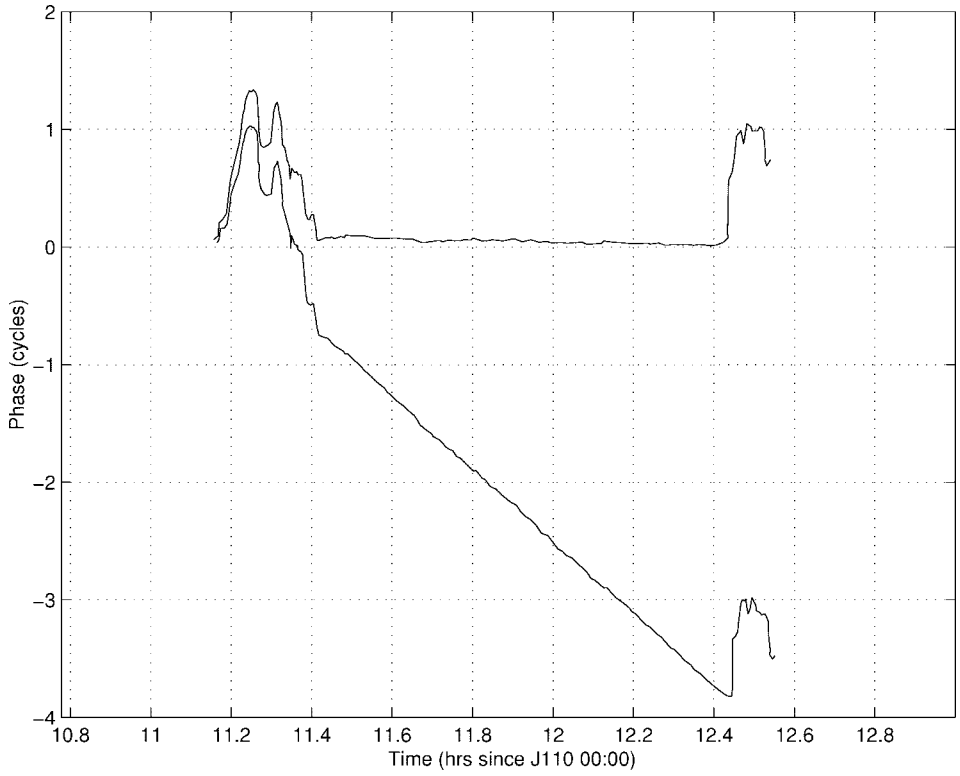


(a)

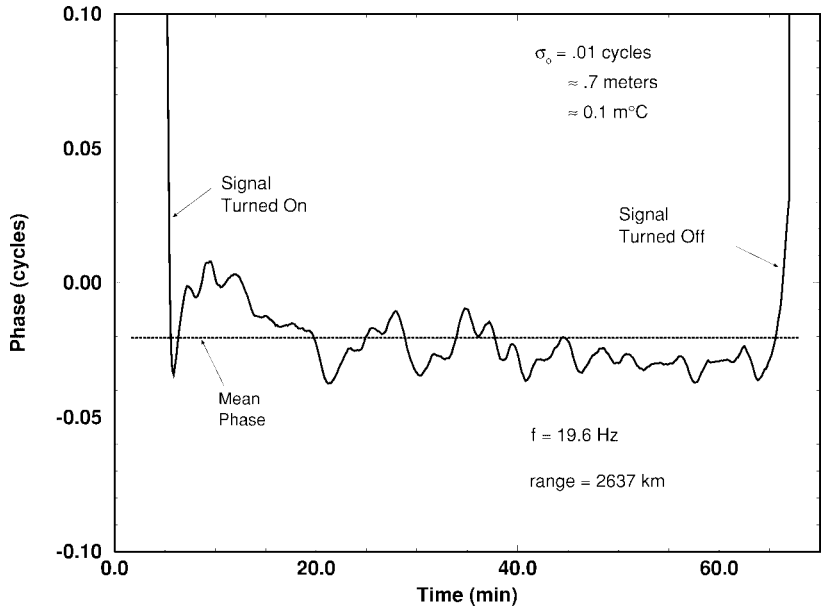


(b)

Fig. 11. Phase stability of CW transmissions from Turpan after compensation for range changes due to the camp drift of Turpan and SIMI for the 1100Z–1200Z April 20 CW transmission. (a) Acoustic phase before and after range phase compensation for the 1-hr transmission. (b) Expanded view of the compensated phase showing the fluctuations which are consistent with a standard deviation predicted by the in-band noise.

using standard time-delay tomography [3]. The standard deviation of the location of the peak is given by

$$\sigma_t \approx \frac{\sqrt{3}}{\pi q F_{\text{eff}}} \tag{1}$$

where $q^2 = 2S/N$ and $F_{\text{eff}}$ is the effective bandwidth. The effective bandwidth of the $M$-sequences is approximately $1/T$, where $T$ is the duration of a single digit of the $M$-sequence, which for TAP was approximately 0.64 s for the 12.5 cycles per digit sequences at 19.6 Hz.

The relative travel time from pulse to pulse was also measured by converting the phase to travel time. It is well known [22] that the standard deviation of the phase estimates, expressed in radians, is related to the SNR by $\sigma_\phi = 1/q$. Converting to the time domain, $\sigma_{t(\phi)} = 1/2\pi f_o q$. Fig. 16 shows the travel-time deviations for mode 3 using direct travel

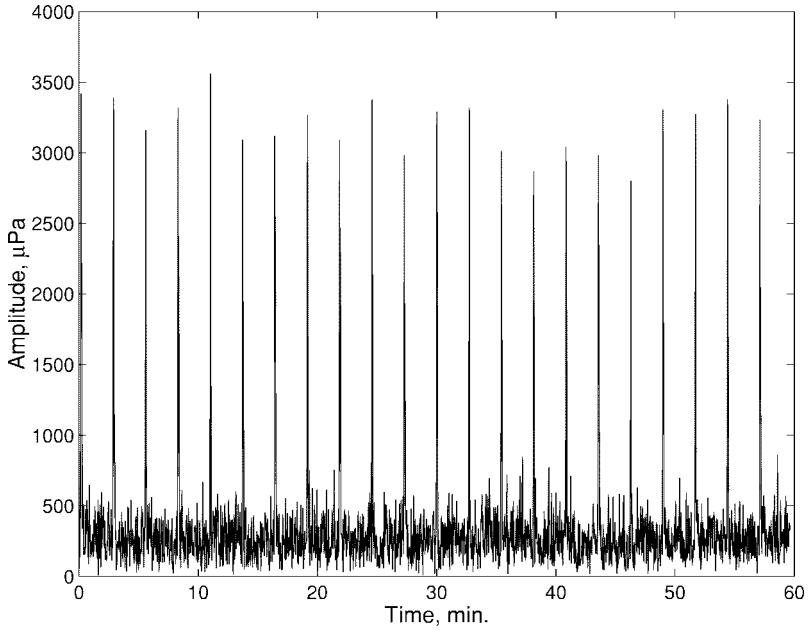


Fig. 12. Single-channel pulse-compressed output for 1 h of an MLS transmission for a 60-m-deep hydrophone of the HA. Each spike represents one sequence period of the MLS transmission.

time measurement and the phase measurement for the twenty two 255 MLS arrivals for transmission #23 shown in Fig. 12. Following the analysis in [19], the SNR for a single arrival for mode 3 (shown in Fig. 13) is approximately 21 dB. From the formulas above $\sigma_t \approx 22$ msecs, and $\sigma_{t(\phi)} \approx 0.5$ ms in excellent agreement with the measurements (Fig. 16). The phase measurement agrees closely with the CW result shown in Fig. 11(b), which is also consistent with the theory. The phase measurement is 40 times more accurate than the direct travel-time measurement. As discussed in Section III-A, if the modes can be resolved either through time dispersion or spatial modal filtering using a VLA, the phase measurement is preferable. Analysis of the travel-time perturbations due to mode coupling on the Turpan-to-Narwhal path [33] have also shown that the phase measurement is more robust in the presence of mode coupling. The disadvantage of the phase measurement is the necessity to resolve any cycle ambiguities from one transmission to the next. This issue will be discussed further in Section IV. In Table I, the first row (TAP data) shows the average arrival time and standard deviation of arrival times for each mode from all 12 sets of MLS's (8 in the case of mode 1), corrected to a reference range of 2637.5 km (the actual range during transmission #23. These were measured directly from the travel-time peaks. The standard deviation is dominated by the manual timing errors discussed above and by the navigation errors. With automatic GPS synchronization, and fixed sources and receivers as planned for the ACOUS program, the travel-time measurements are expected to be better than the single-pulse TAP results reported above.

*2) Travel-Time Modeling Results:* The next rows in Table I indicate the predicted arrival times based upon the coupled normal mode acoustic propagation code discussed earlier [20], [21] at the reference range of 2637.5 km. (The coupled-mode code was needed because of the mode conversion at the Lomonosov Ridge.) The predicted arrival times of each of

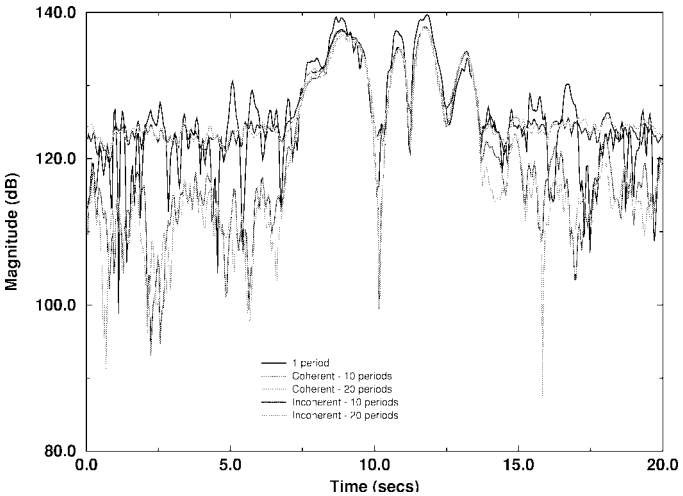


Fig. 13. A single period of the pulse-compressed M255 sequence (black line), incoherent averaging of 10 and 20 periods (blue and light purple lines, respectively), and coherent averaging of 10 and 20 periods (red and green lines, respectively) for the 1-h transmssion.

the modes used three different sets of 26 SVP's along the TAP propagation path from Turpan to SIMI (Fig. 1). The $\Delta$'s are the differences in seconds between the mean of the observed TAP travel times and the model results. The three models used for the 26 SVP's were the following.

- The GDEM set was produced by the Naval Oceanographic Office from data collected by the U.S. Navy in the Arctic through the 1970's and early 1980's [11]. These data represent the historical climatology. For each of the 26 points along the TAP path, the GDEM SVP from the appropriate province was used.
- The AO'94 set was constructed using data taken by a joint U.S. and Canadian icebreaker cruise across the Arctic Ocean in August 1994 (see Fig. 1) [16]. The AO'94 cruise

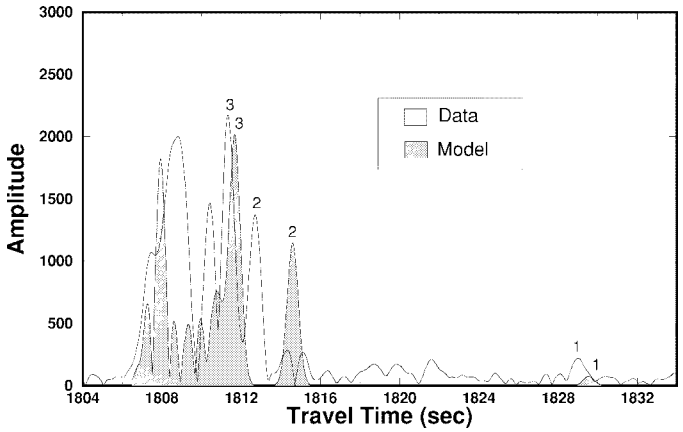


Fig. 14. Beamformed, pulse-compressed, and period-averaged output for the HA and the predicted signal using a range-dependent coupled-mode model. All hydrophones were at 60 m.

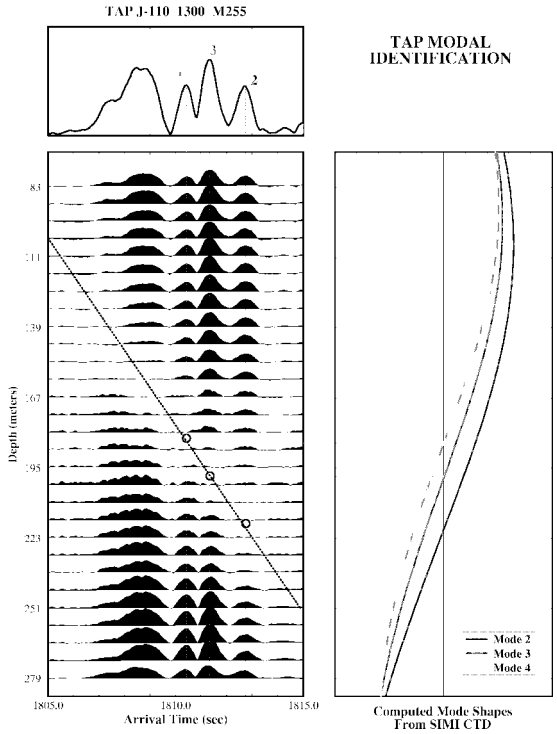


Fig. 15. Pulse-compressed and period-averaged output of the VLA hydrophones showing the measured and predicted zeros for the modal amplitude as a function of depth.

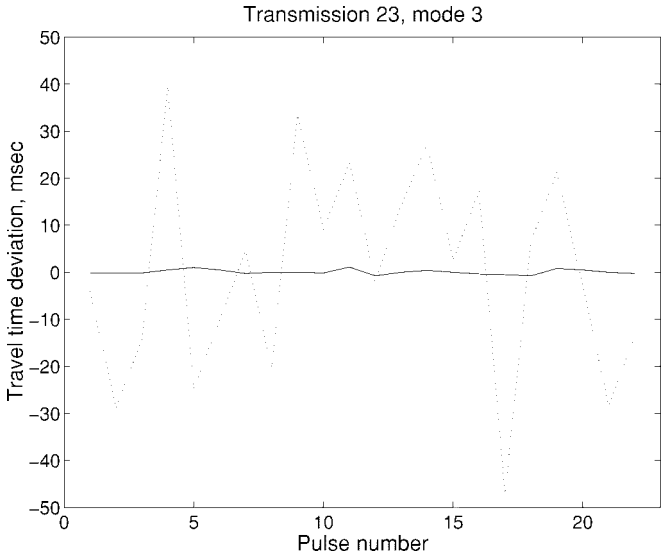


Fig. 16. Changes in travel time of mode 3 measured by the modal arrival times (dotted) and phases (solid) in twenty-two 255 MLS arrivals of transmission #23. The standard deviation of the modal arrival times (dotted) is 22.6 ms, and 0.55 ms for the phase (solid).

TABLE I
ABSOLUTE MODAL TRAVEL TIME SECONDS FOR THE TAP DATA AND THREE OCEANOGRAPHIC MODELS. FOR THE TAP DATA, THE ± INDICATES THE VARIANCE IN THE ESTIMATES DUE TO BOTH THE TIME SYNCHRONIZATION AND THE VARIABILITY OF THE 12 MLS TRANSMISSIONS. FOR THE THREE MODELS, THE Δ INDICATES THE DEVIATION FROM THE MEAN OF THE TAP DATA

| | Mode 1 | Mode 2 | Mode 3 | Mode 4 |
|---|---|---|---|---|
| TAP data | 1828.2 ±1.1 | 1812.2 ±1.2 | 1810.7 ±1.3 | 1809.6 ±1.0 |
| GDEM model | 1829.2 Δ +1.0 | 1814.5 Δ +2.3 | 1811.3 Δ +0.6 | 1810.5 Δ +0.9 |
| AO '94 model | 1828.3 Δ +0.1 | 1812.1 Δ -0.1 | 1811.4 Δ +0.7 | 1810.6 Δ +1.0 |
| AO/SCI model | 1828.7 Δ +0.5 | 1813.4 Δ +1.2 | 1811.6 Δ +0.9 | 1810.7 Δ +1.1 |

did not go into the deeper parts of the Beaufort Sea except for one station, so this one station was used for most of the Beaufort Sea in this set.

- The AO/SCI set consists of a combination of the AO'94 SVP's for the eastern Arctic and just across the Lomonosov Ridge, and SVP's obtained from the SCICEX'95 submarine cruise in April 1995 (Fig. 1) for the Beaufort Sea. For both the AO'94 set and the AO/SCI set, the actual SVP's measured at Turpan and SIMI were used.

The AO'94 set yielded modeling results closest to the TAP data across all four modes. The AO/SCI is quite close to the GDEM climatology for modes 1, 3 and 4; however, it predicts a faster mode 2 than GDEM and is closer to the TAP data. The consistent offset of modes 3 and 4 from the data for all three sets of SVP's could indicate that there is an unknown offset in the TAP data of 0.8–0.9 s. Since the deeper waters are presumably more stable, and since modes 3 and 4 sample these deeper waters (>700 m), agreement should be better. Simply adding an offset of 0.6 s to all TAP travel times would be equivalent to shifting the average temperature by 0.15 °C. Even with adding this offset, mode 2 from TAP is still over 1.5 s faster than that predicted by the climatology, which supports the interpretation that the AIW layer in the eastern Arctic has warmed over the last five and ten years.

The modal interarrival times from the 12 MLS transmissions were calculated from travel time peaks. This provides a

TABLE II
INTERARRIVAL TIMES OF THE TAP MODES AND THE DIFFERENCES COMPARED WITH THE PREDICTED INTERARRIVAL TIMES FROM THE GDEM CLIMATOLOGY AND THE TWO MORE RECENT SVP MEASUREMENTS

| | Modes 1-2 | Modes 2-3 | Modes 3-4 |
|---|---|---|---|
| TAP data | 16.21 ±0.15 | 01.48 ±0.11 | 00.87 ±0.07 |
| GDEM model | 14.71 Δ +1.50 | 03.22 Δ +1.74 | 00.77 Δ -.10 |
| AO '94 model | 16.13 Δ -0.08 | 00.68 Δ -0.80 | 00.76 Δ -0.11 |
| AO/SCI model | 15.39 Δ -0.82 | 01.73 c Δ +0.25 | 00.93 Δ +0.06 |

more robust comparison since this measure is independent of absolute timing errors from one MLS sequence to the next. These results are shown in Table II. The standard deviations are consistent with theory [see (1)], given the lower SNR's of modes 1, 2, and 4.

When interpreting these results, we note the consistency of the interarrival times from the TAP data as indicated by the small standard deviations. The agreement of the data and all of the models with the interarrival time of modes 3 and 4 indicates consistency of the deeper part of the SVP's in the models with the TAP data, not observed with the absolute travel times. Clearly, both the newer data sets (AO'94 and AO/SCI) are in better agreement with the data for the interarrival times between modes 1 and 2 and between modes 2 and 3. As in Table I, the $\Delta$ is the time difference in seconds of the interarrival times compared with the TAP observations. The difference between the GDEM times and the AO'94 and AO/SCI times is a result of the faster arrival time of mode 2, which is consistent with the observations.

### D. Propagation Loss

Propagation loss was measured for both the Turpan–SIMI and Turpan–Narwhal paths using both the CW and MLS signals. The objective of these measurements was to determine the propagation loss associated with individual modes, which is mainly due to ice scattering as well as bottom scattering at Narwhal.

*1) Turpan–SIMI Path:* The vertical array at SIMI was relatively short, spanning only 60–260 m, so it could not resolve the individual modes of the CW signals using spatial filtering. It also could not measure the entire power flux through the waveguide vertical cross section. An alternative approach was to estimate the mean transmission loss in both horizontal and vertical directions. The horizontal averaging was possible since the range of the Turpan–SIMI path changed during the course of the experiment. Fig. 3 indicates the relative drift of the two ice camps. Fig. 17(a) shows a two-dimensional (2-D)

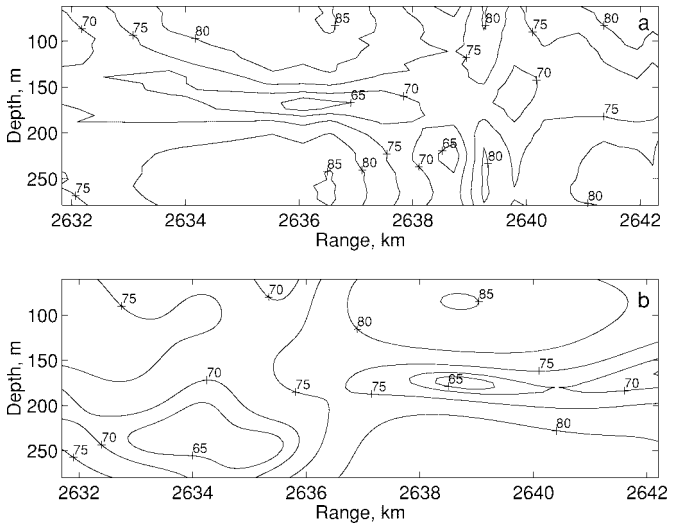


Fig. 17. (a) Measurements of the 2-D distribution of the sound field on the SIMI vertical array for a 10-km drift over two days. (b) Theoretical prediction of the sound field during the same period.

TABLE III
ICE PROPERTIES PHYSICAL PARAMETERS USED FOR MODELING THE ICE SCATTERING ON THE TURPAN–SIMI PATH

| Ice property | Model parameter |
|---|---|
| Density | 910 kg/m$^3$ |
| Compressional speed | 3500 m/s |
| Compressional attenuation | .15 dB/m/kHz |
| Shear speed | 1800 m/s |
| Shear attenuation | 1.0 dB/m/kHz |

distribution of the sound field in a vertical plane obtained from the CW vertical array signals for two days (18 transmissions). During this time, the range changed by approximately 10 km. The measured sound field in Fig. 17(a) demonstrates a horizontal interference structure with many maxima and minima. The most significant feature is a minimum at 170–180 m corresponding to the zeroes of modes 2–4. The signal level averaged over the entire vertical section of the waveguide and the two days of transmissions is approximately 75 dB re 1 $\mu$Pa, which implies an average propagation loss of 120 dB.

Fig. 17(b) shows a theoretical prediction of the sound field at the same range interval as in Fig. 17(a). This prediction was computed using: 1) an adiabatic mode propagation model; 2) an ice scattering model developed by Kudryashov [28]; and 3) the sound-speed profiles along the path calculated from the CTD data from the Arctic Ocean section in 1994 [16]. The ice parameters used for the calculation of the ice scattering loss are given in Tables III and IV. Separate statistics for flat and ridged ice were derived from ice draft data acquired in the Central Arctic Basin and Beaufort Sea by upward echosounders on submarines [30].

TABLE IV
STATISTICAL PARAMETERS OF THE ICE COVER USED FOR MODELING THE ICE SCATTERING ON THE TURPAN–SIMI PATH

| Boundary property | Level ice | Ridge ice |
|---|---|---|
| Fraction | .6 | .4 |
| Standard deviation of lower boundary | 3.0 m | 5.5 m |
| Correlation length of lower boundary | 2.0 m | 3.5 m |
| Standard deviation of upper boundary | .7 m | .7 m |
| Correlation length of upper boundary | 40.0 m | 40.0 m |
| Roughness correlation between boundaries | .7 | .7 |

Although the vertical and horizontal structure of the measured and modeled sound fields are not identical, the signal levels for the maxima and minima as well as the mean are very similar over this 10-km section. There is also the minimum at the 170–180-m depth within approximately 2 km in range, which is consistent with the data. This similarity suggests that the modeled ice scattering loss and the derived modal attenuation coefficients are in agreement along the Turpan–SIMI path. Obviously, the principal reason for disagreement in the interference structure is the difference between the sound speeds during the time of the experiment and those used from the AO data base.

Modes 1–4 in the MLS signals received at SIMI were separated in the time domain by pulse compression, as illustrated in Fig. 14, so modal attenuation loss can be measured directly from the estimated magnitude of each mode. Fig. 18 shows the mean values and standard deviations of the path average estimates of the measured attenuation coefficient of modes 1–4. The theoretical prediction of the attenuations based upon the same model by Kudryashov [28] are also indicated, and they agree quite closely with the experimental estimates. Note that the larger standard deviation on the estimate of mode 1 is due to the lower SNR, while the deviations in modes 2–4 were mainly due to the overlap interference of these modes. For comparison, the horizontal dashed line in Fig. 18 indicates the attenuation of a 19.6-Hz signal in the Arctic waveguide, as calculated by DiNapoli's [32] empirical fit.

*2) Turpan–Narwhal Path:* The path from Turpan to Narwhal was shorter than that for Turpan to SIMI, ≈1000 km versus ≈2600 km; however, the Narwhal site was in the shallower water of the contintental margin, which impacted the received modal pattern. The receptions at Narwhal have been reported separately by Pawlowicz *et al.* [10]. Here, the same analysis that was used for the Turpan–SIMI path is applied for comparison. Fig. 19 shows a waveform of the pulse-compressed MLS signal received on a single hydrophone at 182-m depth in the Narwhal VLA. Because the path is shorter, modes 2–4 are not as well separated in time from each other in addition to some higher order modes. Modes 2 and higher are contained in the first arrival while mode 1

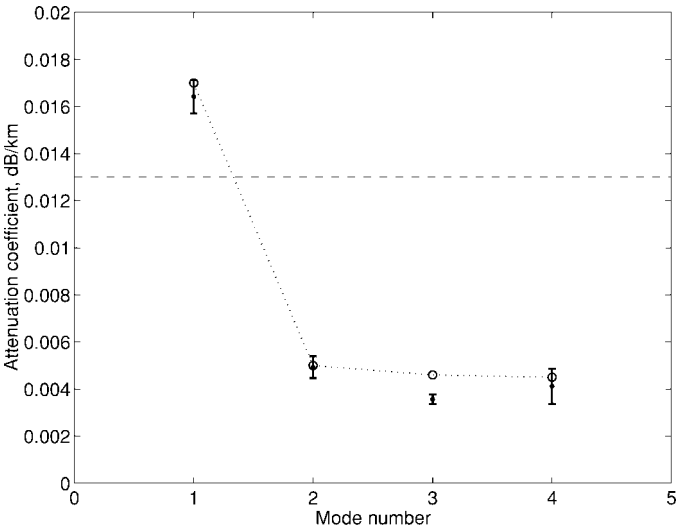


Fig. 18. Attenuation coefficients for modes 1–4. The circles are the model results, the black dots with error bars are the estimates from the TAP data, and the dashed line is from DiNapoli's empirical fit.

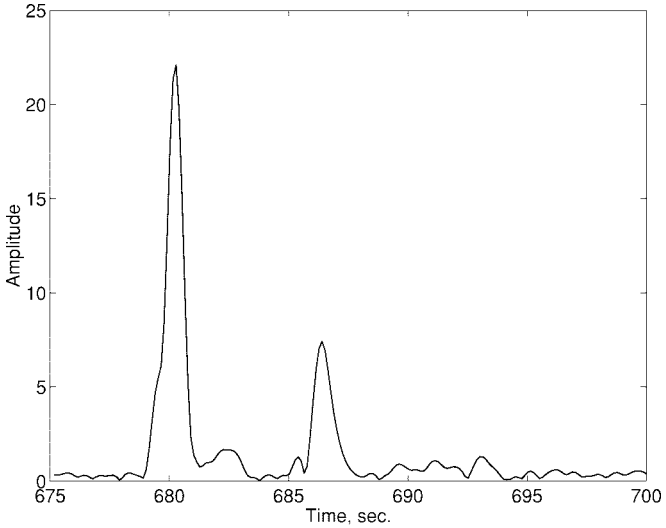


Fig. 19. Received MLS signal (transmission 19) at Narwhal on a hydrophone at a depth of 182 m.

arrived 6 s later at a lower power level. Modal filtering of the VLA data was used to separate the modes in both the CW and MLS signals. This was more effective at Narwhal than at SIMI because the Narwhal VLA spanned the entire water column. The accuracy of modal filtering is very sensitive to errors in the array shape, so array element location (AEL) using high-frequency pingers is needed to compensate for the VLA deformation. Only data supported by AEL tracking was processed [33].

The estimates of the mean modal amplitudes from four transmissions are shown in Fig. 20. The error bars on one of the curves indicate the standard deviation of that transmission which is illustrative of the error in the estimates and those of the others are of the same order. Note that the variation of the modal amplitudes among transmissions exceeds the standard deviations of the individual ones. The most probable origin of such a variation is long-term changes in the mode

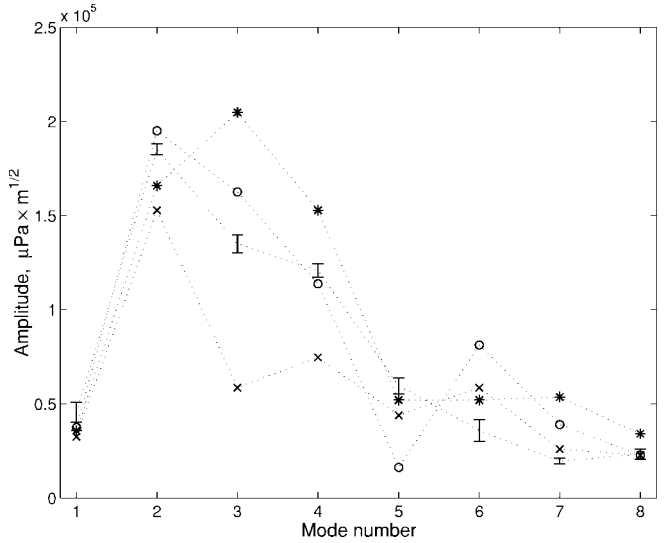


Fig. 20. Received MLS modal amplitudes after mode filtering for four transmissions. The transmission with the error bar is indicative of the standard deviation in the sequence averaging for one of the transmissions.

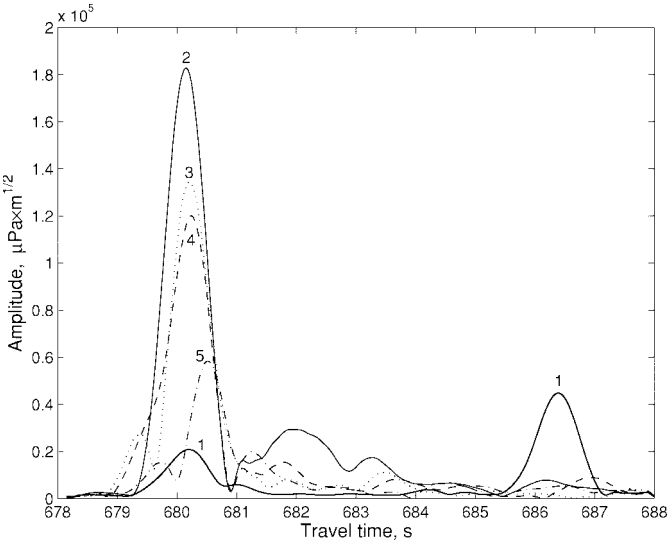


Fig. 21. Received MLS arrivals at Narwhal after modal filtering.

coupling across the continental margin due to changes in the source/receiver distance [33].

The VLA at Narwhal spanned most of the water column, so array processing using modal matched filtering can be employed to separate the modes. This is accomplished by weighting the elements of the VLA proportional to each mode amplitude at the receiver. Since the "$Q$" of the source is high, the proportional bandwidth of the signal is low. Consequently, just one set of weights for the modes at the carrier frequency of 19.6 Hz are needed. Fig. 21 indicates the mode filter outputs for one of the transmissions. Modes 2–5 arrive at the same time. Mode 1 has two prominent peaks; one is coincident with the higher order modes while the second is approximately 6 s later. The time of the second arrival agrees with the time from an adiabatic mode propagation prediction code. The earlier arrival can be attributed to modal coupling from the higher order modes into mode 1 across the continental margin or modal crosstalk in the spatial filtering.

Modes for the CW signals can also be separated using least mean square (LMS) spatial filtering on the VLA. This is similiar to modal matched filtering except that the covariance of the received signal across the array and the mode weights at the carrier frequency are used. Fig. 22 indicates the estimates of modal amplitudes and their standard deviations averaged over the twelve CW transmissions where AEL positioning was available. The standard deviations, which are much greater than those with each 1-h transmission, suggest an instability among the transmissions. Note the modal amplitudes are greater by roughly a factor of two, which is a consequence of the 3-dB difference between the level of the CW and the level of the MLS signals after removal of the carrier component.

A cumulative estimate of the attenuation of the modes on the Turpan to Narwhal path, indicated in Fig. 23 (dotted line), were determined by averaging the modal amplitude estimates of the four MLS and twelve CW transmissions used above. Also shown is the cumulative estimate of the attenuation for the Turpan-to-SIMI path (dashed line) for modes 1–4. The

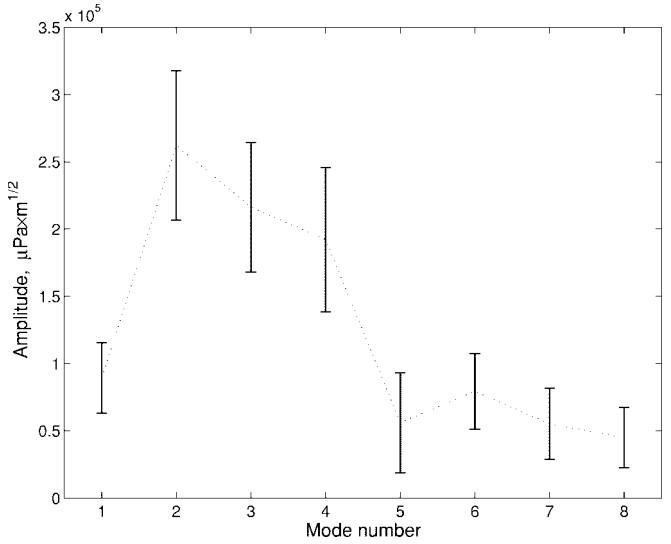


Fig. 22. Received CW average modal amplitudes after modal filtering. The error bars indicate the variance of the envelope over the 12 1-h transmissions.

path lengths differed by a factor of approximately 2.5. If the attenuations were simply due to geometrical spreading in the $10\log(R)$ part of a transmission loss curve, the difference in attenuation should have been approximately 4 dB, which is of the same order of magnitude as the standard deviations of the estimates. The attenuation estimates for modes 2–4 are of this order. Mode 1, however, differs by roughly 16 dB. This can be explained by noting that mode 1 interacts most strongly with the ice, and this attenuation in decibels increases linearly with range, causing the much higher attenuation difference for mode 1. There is also a rather complicated bottom interaction factor associated with the Turpan–Narwhal path since Narwhal was in shallow water. The shoaling bathymetry leads to bottom interaction for these modes which introduces additional attenuation that would offset the lower geometric spreading loss for this path compared to the Turpan–SIMI path. This, perhaps, is suggested by the higher attenuation for modes 3 and 4 for the Turpan–Narwhal path shown in Fig. 23.

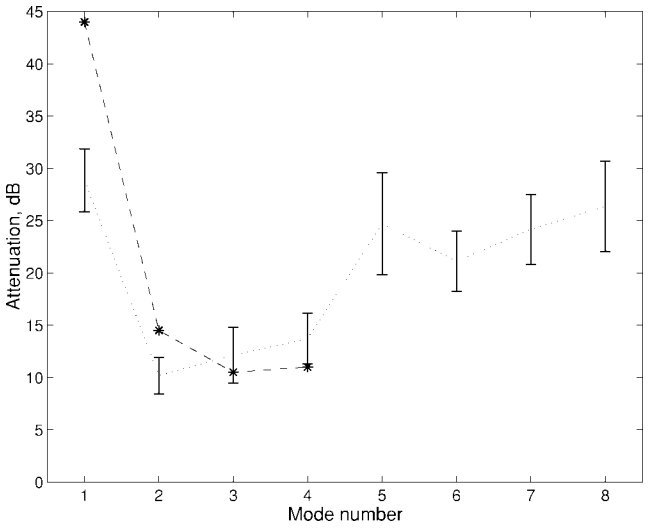


Fig. 23. Comparison of of the estimated modal attenuations using four MLS and 12 CW transmissions. Turpan to SIMI: dashed line; Turpan to Narwhal: dotted line.

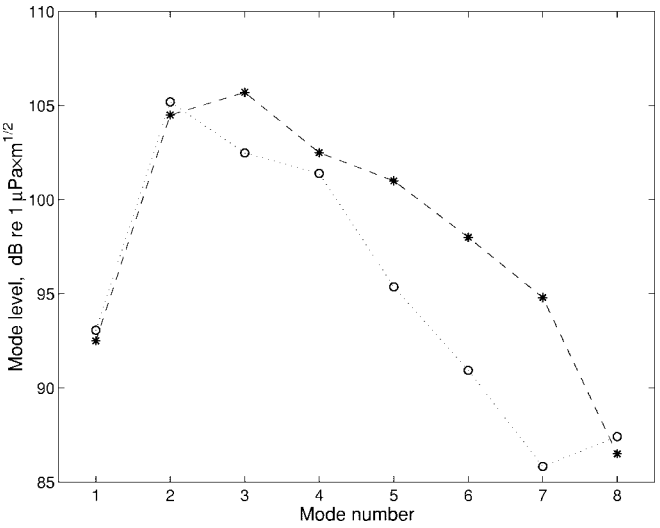


Fig. 24. Comparision of the predicted (stars) and estimated (circles) modal attenuations for the Turpan-Narwhal path.

TABLE V
STATISTICAL PARAMETERS OF THE ICE COVER USED FOR MODELING THE ICE SCATTERING ON THE TURPAN–NARWHAL PATH

| Sect. No. | $L_n$ (km) | $\bar{m}$ (m) | $\sigma_b$ (m) | $\sigma_s$ (m) | $\rho_{b,s}$ (m) |
|---|---|---|---|---|---|
| 1 | 380 | 4.0 | 2.7 | 0.7 | 40. |
| 2 | 100 | 4.0 | 2.7 | 0.7 | 40. |
| 3 | 120 | 5.0 | 3.3 | 0.8 | 40. |
| 4 | 150 | 5.5 | 3.6 | 0.9 | 40 |
| 5 | 215 | 6.0 | 4.0 | 1.0 | 35 |
| 6 | 15 | 6.5 | 4.3 | 1.1 | 35 |
| 7 | 11 | 6.5 | 4.3 | 1.1 | 35 |

$L_n$: section length; $\bar{m}$: mean ice thickness; $\sigma_b$: rms roughness of the bottom; $\sigma_s$: rms roughness of the surface; $\rho_{b,s}$: correlation length of surface and bottom.

We can compare the modal attenuation from the data to that from a numerical propagation model for the Narwhal data, since the modes can be well resolved spatially with the VLA. The propagation model used the same ice scattering model by Kudryashov [28]; the model parameters for the ice were derived from AARI Ice Climatology Atlas [29] and the acoustic properties of the bottom were from Geddes [34]. (The propagation path was divided into sections corresponding to different ice and bottom properties.) The ice properties used are shown in Table V.

Fig. 24 compares the predicted (stars) and estimated (circles) modal attenuation for one of the MLS transmissions. The poorer agreement for modes 5 and higher most likely reflects innacuracies in the model for the bottom properties. The good agreement for the lower order modes, particularly for modes 1 and 2, which interact most strongly with the ice cover, supports the observation that monitoring changes in the modal attenuation can be used to invert for changes in the ice properties.

## IV. CLIMATE MONITORING IN THE ARCTIC

It is widely accepted today that the Arctic is undergoing large changes in both the atmosphere and the ocean and that these changes have an anthropogenic fingerprint [23]. The TAP experiment was the first basin-scale observation which suggested warming in the Arctic Ocean of the Atlantic Layer [1], [4], [5]. In 1993, the cruise of the USS Pargo [24] and the cruise of the CCGS Henry Larson [15], [6] revealed a shift in the boundary between the warmer more saline Atlantic water and the Pacific water toward the Alpha and Mendeleyev Ridges, and warmer water in the Makarov Basin, respectively. The Arctic Ocean Section of the USCGS Polar Sea and the CCGS Louis S. St Laurent (see Fig. 1) conducted in August 1994 confirmed these results [16]. Whether these results are a manifestation of a secular global climate change trend or a natural oscillation of unknown period is an area of active research today. Recent modeling by Proshutinsky and Johnson has suggested that major shifts in the Arctic Ocean circulation occur on a decadal time scale between two dominant circulation regimes [25]. Their models indicate that a regime shift could be occuring now. This shift, which is characterized by a weakening and contraction of the anticyclonic Beaufort Sea gyre, and a corresponding strengthening of cyclonic circulation in the East Siberian and Laptev Seas, with a movement of the Transarctic Drift Current toward the Beaufort Sea, could possibly explain some of the observed changes. A recent analysis of 400 years of paleoclimate records from lake sediments, trees, glaciers, and marine sediments in the Arctic shows that natural variability is large but also makes a case for the dominant influence of the increasing levels of greenhouse gases on Arctic atmospheric warming (+0.6 °C) since 1920 [23]. This increase of Arctic atmospheric temperature exceeds that of the hemisphere as a whole during this period and is consistent with climate models which indicate that the Arctic is a precurser to and amplifies global climate change [26], [27]. In addition to atmospheric warming, the climate modeling also shows a secular increase in Arctic Ocean temperature. Overpeck and

his colleagues conclude that large natural variability coupled with anthropogenic forcing (through increased concentrations of greenhouse gases) are driving "unprecedented changes in the Arctic environment" [23].

Despite the well-understood importance of the Arctic climate's role in the Earth's global climate system and its role as a sensitive indicator of global climate change, something as fundamental as the relative importance of thermohaline forcing and wind-driven forcing on the circulation of the Arctic Ocean remain poorly understood [25]. Understanding the complex feedback mechanisms and external forcing at work in the Arctic that drive its natural variability and determine its response to greenhouse warming are hampered in large part by a lack of synoptic field measurements with incomplete and undersampled records in time. Acoustic thermometry can be a key part of a long-term Arctic Ocean monitoring strategy.

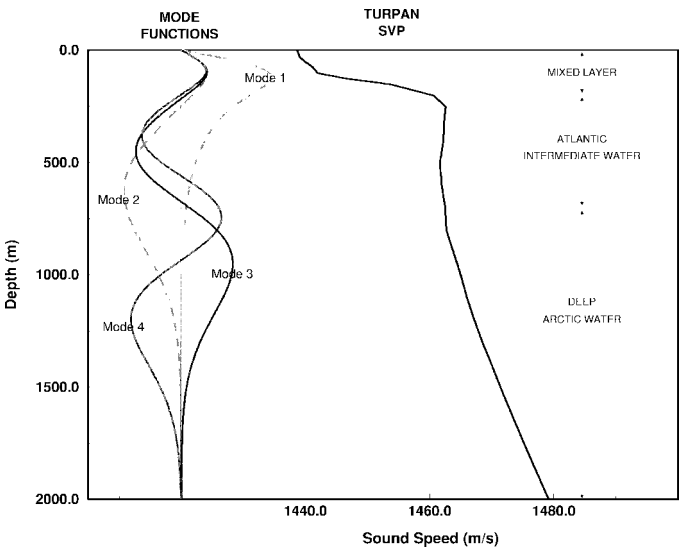


Fig. 25. Acoustic normal modes 1–4 for the sound-speed profile taken at Camp Turpan.

### A. Acoustic Thermometry and Oceanography in the Arctic

Acoustic thermometry is uniquely suited to the Arctic Ocean, despite a complex scattering interaction with the Arctic sea ice. The upward-refracting sound-speed profile generates a modal structure in which successively higher modes sample deeper and deeper depths. The Arctic Ocean is vertically stratified into three major water masses. An upper mixed layer characterized by near freezing temperatures and low salinity created by seasonal summer ice melt and freshwater input from river runoff overlays a sharp halocline and thermocline, marking the transition to the warmer saline waters of Atlantic origin (the AIW) that flow into the Arctic via the Fram Strait and, to a lesser extent, via the Barents Sea and the Santa Anna Trough east of Franz Josef Land. Underlying this AIW is deep Arctic water characterized by the same salinity of the AIW but with decreasing temperatures with increasing depth. The AIW circulates through the entire Arctic Ocean at depths typically between 150–400 m in the eastern Arctic basins to 200–700 m in the Canada basin. The upper mixed layer acts as a cap over the AIW, preventing vertical heat flux to the Arctic sea ice, thereby preserving the Arctic ice cap. A reduction in freshwater input to the Arctic or increasing heat flux from the AIW as result of warmer Atlantic temperatures or increased flow rates into the Arctic could weaken this upper Arctic ocean stratification and lead to a catastrophic reduction of the ice cap. Fig. 25 shows the amplitudes of acoustic modes 1–4 at 19.6 Hz, the sound-speed profile measured at Camp Turpan during the TAP experiment using a CTD, and the major Arctic water types. As discussed earlier in this paper, mode 1 at 19.6 Hz is trapped in the upper Arctic mixed layer. Mode 2 is most sensitive to temperature changes of the AIW, while modes 3 and 4 are most sensitive to changes in the Arctic deep water [18].

*1) Detecting Interannual and Climate Variability:* In Section II-C, it was shown that the measurement of the modal phases using the time-dispersed MLS arrivals provided travel-time change measurements from one transmission to the next with errors of approximately 0.5 ms. However, in order to track travel-time changes with phase, it is necessary to keep track of any whole number cycle changes between transmissions, or, alternatively, it needs to be demonstrated that the change in phase from one transmission to the next will be less than one cycle. This means that the travel time from transmission to transmission must be less than approximately 50 ms. To estimate possible travel-time changes, Russian data from the POLEX [12] series of experiments from 1974 to 1979 were analyzed [18] to determine the interannual variability along a trans-Arctic section very close to the TAP track and the proposed ACOUS track. This analysis included calculation of the consequent modal travel-time variability for modes 1–4. The interannual variability was greatest as expected in the upper Arctic mixed layer with temperature changes up to 0.2 °C. These interannual changes, however, were shown to change the travel time of mode 2 by only 80 ms. This implies a travel-time change of 0.22 ms per day. The planned ACOUS transmission schedule is once every four days, which would give a travel-time change of less than 1 ms. Furthermore, the data were used to compute the change in modal travel time over these years with a hypothesized intrusion of warmer AIW of 0.02 °C per year (consistent with the climate modeling of Manabe *et al.* [26]) at 300 m, decreasing to 0 °C at 200 m and at 1000 m [18]. This resulted in a travel-time decrease for modes 2–5 of 0.45, 0.23, 0.17, and 0.1 s, respectively, over the five years from 1974 to 1979, or 90 ms per year for mode 2. We can compare this hypothesized trend with the recent changes that have been observed in the Arctic Ocean summarized by Morison [24] and with the measured TAP travel times. The TAP data compared with the modeling using climatology indicate as much as a 2-s travel-time decrease in the mode 2 travel, as discussed in Section II. Recent hypotheses are that these changes in the AIW possibly occured over approximately five years in the late 1980's into the early 1990's [24]. This yields a trend of 0.4 s/yr or a little more than 1 ms per day, which is still an order of magnitude less than a wavelength every four days, but an order of magnitude greater than the 0.5-ms resolution of the phase.

*2) An Acoustic Monitoring Grid in the Arctic:* TAP has shown that acoustic thermometry has the resolution to detect

observed and hypothesized changes in the temperature of the Arctic Ocean. With the installation of sources and receivers in the Arctic, a real-time synoptic monitoring capability could be realized. The measurements are high resolution in time and, with many source–receiver paths, could realistically achieve spatial resolution to approximately 100 km×100 km. If such a system had been in place in the 1980's, the recent movement of Atlantic water would have been detected and could have provided timely information for icebreaker and ice-camp-based operations for more detailed analysis.

The ACOUS project installed the first acoustic source in the Arctic Ocean on October 9, 1998, at 81°55.88′N and 38°43.94′E near the shelf break at the edge of the Franz Victoria Strait between Franz Josef Land and the Svalbard Archipelago. The source transmits 10 MLS 255-digit sequences at a center frequency of 20.49 Hz, 10 cycles per digit, yielding a total signal duration of approximately 20.74 min. Each transmission starts at 0000 GMT every four days. The first regular transmission was at 0000 GMT on October 15, 1998. The source is battery-powered and designed for a life of 2.5–3 years. It is moored from the bottom with the source at a depth of 60 m below the surface. An autonomous acoustic receiving array was installed in the Lincoln Sea on October 1, 1998, at 84°3.4′N and 66°25′W, in 545-m water depth. There are eight hydrophones spaced at 70-m intervals starting at 12 m from the bottom. There are five microCTD's that record temperature and salinity every 10 min at 14, 326, 434, 467, and 507.4 m from the bottom. The array records the acoustic data from 18 Hz to 22 Hz for 2 h every four days, synchronized with the source transmissions. An array is being fabricated for installation in the Beaufort Sea off Pt. Barrow, Alaska, in the fall of 2000. This array will be cabled back to shore and will provide real-time data. A second source is planned for installation in the central Arctic Ocean on the Lomonosov Ridge.

These first sources and receivers will provide a protoype monitoring grid expandable to a multiple source receiver system envisioned above that can cover the entire Arctic basin, sending data back in real time. The cabled nodes can also serve as ocean observatories supporting moored instruments and as receiving stations for downloading data and recharging batteries for autonomous vehicles performing targeted continuous high-resolution sampling of oceanographic, chemical, biological, and sea ice processes.

The recent measurements of increased temperature in the AIW layer of the Arctic Ocean from icebreakers and submarines are consistent with the observed modal travel times of the TAP experiment in April 1994. Whether this is a "normal" cyclical phenomena or an indicator of a long-term secular trend is unknown. Data from the Arctic Ocean are badly aliased in both time and space, making definitive evaluation of even interannual cycles difficult. The need for a system for synoptic continuous and real-time monitoring is evident. Acoustic thermometry can provide such a capability.

## APPENDIX A

The TAP transmissions used MLS sequences for determining travel times as have been used in most tomography experiments [31]. The signal is given by

$$s(t) = \sqrt{2P}\cos(2\pi f_o t + m(t)\Delta\Theta) \tag{2}$$

where $P$ is the transmitted power (195 dB re 1 $\mu$Pa at 1 m, or 251 W), $f_o$ is the carrier frequency (19.6 Hz), $m(t)$ is the MLS sequence which has levels of $\pm 1$, and $\Delta\Theta$ is the phase deviation of the modulation. The modulating sequence $m(t)$ shifts levels at a chip interval $T$ which is usually designated in terms of cycles $L$ of the carrier, or $T = L/f_o$; it is periodic with a sequence length $NT$, where $N$ is the number of digits. For the TAP experiment, the bandwidth of the source permitted digit lengths with $L = 25$ and 12.5 cycles. (The faster rate was used after it was determined *in situ* that the source had sufficient bandwidth.) Sequence lengths of $N = 127, 255, 511$ and 1023 digits were used. Fig. 6 illustrates a complex (I/Q) demodulation of the signal from a nearby source monitor. The signal is repeated periodically such that $K$ periods, or sequences, were transmitted during the 1-h transmission interval.

MLS sequences are used because of their good autocorrelation properties. It can be demonstrated that the complex output of a correlator using a single period of the MLS as a replica is given by

$$C(\tau) = \sqrt{P}\left[\left(\cos^2(\Delta\Theta) - \frac{1}{N}\sin^2(\Delta\Theta)\right) + \left(\left(1 + \frac{1}{N}\right)\sin^2(\Delta\Theta)p(\tau)\right)\right] \tag{3}$$

where $p(\tau)$ is a triangular pulse given by

$$p(\tau) = \begin{cases} 1 - \dfrac{|\tau|}{T}, & |\tau| \le T \\ 0, & |\tau| > T \end{cases}$$

In practice, only a finite number of sequences are transmitted, so the correlation over the first and last sequences are degraded. The first term in (3) represents power left in the carrier unless $\Delta\Theta = \tan^{-1}(\sqrt{N})$ [31]. In the TAP experiment, $\Delta\Theta = \pi/4$, so approximately one half the power was in the carrier.

If we ignore the power in the carrier, which simply leads to an amplitude offset, the coherent output of the correlator for the $k$th sequence for each mode $m$ is given approximately as follows:

$$l_m(\tau) = \sqrt{P}\cdot 10^{-\alpha_m R_o/2} p(\tau - p_m R_o) \cdot \exp(-j(2\pi\frac{\dot{R}_o}{\lambda_m}kNT + \phi_m)) \tag{4}$$

where $R_o$ is the nominal source/receiver range (m), $\alpha_m$ is the modal attenuation (dB/m), $p_m$ is the modal slowness (s/m), $\dot{R}_o$ is the nominal source/receiver range rate (m/s), $\delta_m$ is the modal wavelength (m), $kNT$ is the time offset for the $k$th sequence where each sequence is $NT$ s long, and $\phi_m$ is the phase delay for the $m$th mode plus system phase shifts. (All these terms are functions of the center frequency at 19.6 Hz.) The total reception is the sum for each of the modes, or

$$l(\tau) = \sum_m l_m(\tau).$$

The term $\dot{R}_o/\lambda_m kNT$ represents the phase shift across the sequences which needs to be compensated before coherently averaging them. The final output is given by

$$\overline{l}(\tau) = \sum_{k=0}^{K-2} l(\tau - (k+1)NT)$$

where $\tau$ brackets the nominal travel time from the source to receivers (≈680 s for Turpan–Narwhal and ≈1800 s for Turpan–SIMI).

## ACKNOWLEDGMENT

The authors would like to thank Academician A. Gaponov-Grekhov, Director of Institute of Applied Physics (IAP), Nizhny Novgorod, Dr. M, Slavinsky, former Deputy Director of the IAP and leader of the TAP source development group at IAP, and Prof. N. Dubrovsky, Director of the Acoustics Institute in Moscow, for their early and critical support of the TAP Experiment and the ACOUS program in Russia. The authors also want to thank H. Schmidt (MIT), B. Sotirin (NRAD, now Director, CRREL), M. Lents [Sciences Application International Corporation (SAIC)], A. Shmelerv (Institute of General Physics), K. von der Heydt and E. Scheer [Woods Hole Oceanographic Institution (WHOI)], and T. Curtin (Office of Naval Research) for their efforts at the ice camps. The signal analysis was supported by H. Freese (SAIC), Y. Lee (SAIC), A. Mehrabian (SAIC), M. Andreyev (Shirshov Institute), and E. Scheer (WHOI). The VLA was loaned to the SIMI ice camp by G. Duckworth of Bolt, Beranek & Neuman.

## REFERENCES

[1] P. N. Mikhalevsky, A. B. Baggeroer, A. N. Gavrilov, and M. Slavinsky, "Experiment test use of acoustics to monitor temperature and ice in arctic ocean," *EOS Trans. Amer. Geophys. Union*, vol. 76, no. 27, pp. 265–269, July 1995.

[2] _____, "CW and $M$ sequence transmissions across the arctic," *J. Acoust. Soc. Amer.*, pt. 2, vol. 96, no. 5, pp. 3235–3236, Nov. 1994.

[3] W. Munk and C. Wunsch, "Ocean acoustic tomography: A scheme for large scale monitoring," *Deep Sea Res.*, vol. 26, pp. 123–161, , 1979.

[4] P. N. Mikhalevsky, A. N. Gavrilov, and A. B. Baggeroer, "Are faster than predicted signals seeing arctic ocean warming?," *J. Acoust. Soc. Amer.*, pt. 2, vol. 97, no. 5, p. 3234, May 1995.

[5] P. N. Mikhalevsky, R. E. Keenan, and A. B. Baggeroer, "Measured transarctic acoustic travel times and model comparisons," in *Proc. 3rd Eur. Conf. on Underwater Acoustics*, Heraklion, Crete, Greece, June 24–28, 1996, vol. 2, pp. 773–777.

[6] F. A. McLaughlin, E. C. Carmack, R. W. MacDonald, and J. K. B. Bishop, "Physical and geochemical properties across the atlantic/pacific water mass front in the southern canadian basin," *J. Geophys. Res.*, vol. 101, no. C1, pp. 1183–1197, Jan. 15, 1996.

[7] M. Steele and T. Boyd, "Retreat of the cold halocline layer in the arctic ocean," *J. Geophys. Res.*, vol. 103, no. 55, pp. 10419–10435, May 15, 1998.

[8] Defense Mapping Agency Technical Report 8350.2, "Department of defense world geodetic system 1984," 2nd ed., U.S. Geological Survey, Denver, CO, Sept. 1, 1991.

[9] M. Slavinsky, B. Bogolyubov, I. Alelekov, K. Pigalov, J. L. Spiesberger, and P. Boutin, "Evaluation of electromagnetic source for ocean climate acoustic thermometry at Lake Seneca," WHOI Rep. 93-09, Woods Hole Oceanographic Insitution, Feb. 1993.

[10] R. Pawlowicz, D. Farmer, B. Sotirin, and S. Ozard, "Shallow-water receptions from the transarctic acoustic propagation experiment," *J. Acoust. Soc. Amer.*, vol. 100, no. 3, pp. 1482–1492, Sept. 1996.

[11] W. J. Teague, M. J. Carron, and P. J. Hogan, "A comparison between the generalized digital environment model and levitus climatologies," *J. Geophys. Res.*, vol. 95, pp. 7167–7183, 1990.

[12] K. D. Sabinin and S. V. Pisarev, "Oceanographic background to the arctic ATOC feasibility study,"—in Acoustic Monitoring of the Arctic Ocean Climate: Feasibility Research and Modeling Prepared for SAIC, AcoustInform Report 94/04, pp. 1–40, 1994.

[13] Naval Oceanographic Office Data Model DBDB-V. 1998. [Online]. Available WWW: http://128.160.23.42/dbdbv/database_doc.html

[14] P. N. Mikhalevsky, "Characteristics of CW signals propagated under the ice in the arctic," *J. Acoust. Soc. Amer.*, vol. 70, no. 6, pp. 1717–1722, Dec. 1981.

[15] E. C. Carmack, R. W. Macdonald, R. G. Perkin, F. A. McLaughlin, and R. J. Pearson, "Evidence for warming of atlantic water in the southern canadian basin the arctic ocean: Results from the larsen-93 expedition," *Geophys. Res. Lett.*, vol. 22, no. 9, pp. 1061–1064, 1995.

[16] E. C. Carmack, K. Aagard, J. H. Swift, R. W. Macdonald, E. P. McLaughlin, E. P. Jones, R. G. Perkin, J. N. Smith, K. Ellis, and L. Kilius, "Changes in temperature and contaminant distributions within the arctic ocean," *Deep Sea Res.*, vol. 4, pp. 1487–1502, 1997.

[17] R. E. Keenan, L. Merriam, M. S. Moustafa, and P. N. Mikhalevsky, "Upper ocean observations across an arctic transect," in *AGU Ocean Science Meeting*, San Diego, CA, Feb. 16, 1997.

[18] A. N. Gavrilov and P. N. Mikhalevsky, "Modeling an acoustic response to long-term variations of water and ice characteristics in the arctic ocean," in *Proc. Oceans 1995 MTS/IEEE*, San Diego, CA, Oct. 9–12, 1995, vol. 2, pp. 941–948.

[19] A. N. Gavrilov and P. N. Mikhalevsky, "Phase acoustic tomography with broadband signals," in *Proc. 3rd Eur. Conf. Underwater Acoustics*, Heraklion, Crete, Greece, June 24–28, 1996, vol. 2, pp. 851–856.

[20] R. B. Evans, "A coupled mode solution for acoustic penetration in a waveguide with stepwise depth variations of a penetrable bottom," *J. Acoust. Soc. Amer.*, vol. 74, pp. 188–195, 1983.

[21] H. A. Freese, "Use of simplified coupled mode propagation for the prediction of impulse responses of megameter trans-arctic propagation paths," *J. Acoust. Soc. Amer.*, pt. 2, vol. 97, no. 5, p. 3234, May 1995.

[22] J. S. Bendat and A. G. Piersol, *Random Data: Analysis and Measurement Procedures*. New York: Wiley, 1986.

[23] J. Overpeck, K. Hughen, D. Hardy, R. Case, M. Douglas, B. Finnery, K. Gajewski, G. Jacoby, A. Jennings, S. Lamooureux, A. Lasca, G. MacDonald, J. Moore, M. Retelle, S. Smith, A. Wolfe, and G. Zielinski, "Arctic environmental change of the last four centuries," *Science*, vol. 278, no. 5341, pp. 1251–1256, Nov. 1997.

[24] J. Morison, "An open letter describing a program for a study of arctic change," personal correspondence, Sept. 1997.

[25] A. Y. Proshutinsky and M. Johnson, "Two circulation regimes of the wind-driven arctic ocean," *J. Geophys. Res.*, vol. 102, no. C6, pp. 12493–12514, June 1997.

[26] S. R. Manabe, R. J. Stouffer, M. J. Spelman, and K. Bryan, "Transient responses of a coupled ocean-atmosphere model to gradual changes of atmospheric $CO_2$, part I: Annual mean response," *J. Climate*, vol. 4, p. 785, 1991.

[27] S. R. Manabe and R. J. Stouffer, "Multiple-century response of a coupled ocean-atmosphere model to an increase of atmospheric carbon dioxide," *J. Climate*, vol. 7, no. 1, pp. 5–23, 1994.

[28] V. M. Kudryashov, "Calculation of the acoustic field in an arctic waveguide," *Phys. Acoust.*, vol. 42, pp. 386–389, 1996.

[29] Environmental Working Group (EWG), *Joint U.S.-Russian Atlas of the Arctic Ocean*, (CD-ROM), National Snow and Ice Data Center, Boulder, CO, 1997.

[30] S. V. Brestkin, E. O. Aksconov, and V. F. Zakharov, "Statistical characteristics of the bottom profile of the arctic ice cover," Tech. Rep. 94/3, Acoustinform, Moscow, Russia, May 1994.

[31] W. H. Munk, P. F. Worcester, and C. Wunsch, *Ocean Acoustic Tomography*. Cambridge, U.K.: Cambridge Univ., 1995.

[32] F. N. DiNapoli and R. Mellen, "Low frequency attenuation in the arctic ocean," in *Ocean Seismo-Acoustics*, T. Akai and J. M. Berkson, Eds. New York: Plenum Press, 1986, pp. 387–395.

[33] A. N. Gavrilov and P. N. Mikhalevsky, "Mode coupling effects in acoustic thermometry of the arctic ocean," *J. Acoust. Soc. Amer.*, submitted for publication.

[34] W. H. Geddes, "Geoacoustic model of the Lincoln Sea," GGAI Tech. Rep. 3-90, Mar. 1990.

**Peter N. Mikhalevsky** received the B.A. and M.S. degrees jointly from Harvard University, Cambridge, MA, in 1972 and the Ph.D. degree from the Massachusetts Institute of Technology (MIT), Cambridge, in 1979.

In 1972, he was commissioned an officer in the U.S. Navy and served on active duty for 12 years. His specialty was Anti-Submarine Warfare and he was instrumental in the introduction of tactical towed arrays in the Navy in the mid-1970's. After the Navy in 1983, he was an Associate Professor in the Department of Ocean Engineering at MIT, teaching acoustics and array processing. He joined SAIC in 1985 and is a Corporate Vice President and Manager of the Ocean Sciences Division in McLean, VA. His work has focused on matched field processing and array processing in the ocean. He is the principal investigator of the Arctic Climate Observations using Underwater Sound (ACOUS) program which is a joint U.S./Russian Gore-Chernomyrdin project using acoustic thermometry to study climate change in the Arctic.

Dr. Mikhalevsky is a fellow of the Acoustical Society of America. For his research in underwater acoustics, he was the recipient of the Biennial Award (now the R. Bruce Lindsay Award) of the Acoustical Society of America, the A. B. Wood Medal and Prize from the Institute of Acoustics, U.K., and the Decibel Award from the Naval Undersea Warfare Center, New London, CT.

**Alexander N. Gavrilov** received the M.S. degree in physics from the Physics Department of the Moscow State University, Russia in 1979, and the Ph.D. degree in acoustics from N. N. Andreyev Acoustics Institute, Moscow, Russia, in 1995.

In 1979, he began working at the N. N. Andreyev Acoustics Institute as a Research Scientist until 1989, and then as a head of the Arctic Acoustics Department until 1996. Since 1996, he has been working as a Senior Research Scientist for P. P. Shirshov Institute of Oceanology, Moscow, Russia, where he is currently managing the project of acoustic thermometry of the Arctic Ocean climate. He has extensive research experience in the field of Arctic acoustics and signal processing.

**Arthur B. Baggeroer** (S'62–M'68–SM'87–F'89) received the B.S.E.E. degree from Purdue University, West Lafayette, IN, in 1963 and the Sc.D. degree from the Massachusetts Institute of Technology (MIT), Cambridge, in 1968.

He is a Ford Professor of Engineering in the Departments of Ocean Engineering and Electrical Engineering and Computer Science at MIT. He has also been a consultant to the Chief of Naval Research at the NATO SACLANT Center in 1977 and a Cecil and Ida Green Scholar at the Scripps Institution of Oceanography in 1990 while on sabbatical leaves. His research has been concerned with sonar array processing, acoustic telemetry, and, most recently, global acoustics and matched field array processing. He also has had a long affiliation with the Woods Hole Oceanographic Institution and was Director of the MIT—Woods Hole Joint Program from 1983 to 1988.

Dr. Baggeroer is a fellow of the Acoustical Society of America, and he was elected to the National Academy of Engineering in 1995. He was awarded the Secretary of the Navy/Chief of Naval Operation Chair in Oceanographic Science in 1998.